Fibers and Polymers (2025) 26:4397–4417
https://doi.org/10.1007/s12221-025-01094-w

Online ISSN 1875-0052
Print ISSN 1229-9197

REGULAR ARTICLE

Evaluation of Deflection–Creep Properties of Sleeve-Retrofitted Pultruded Glass Fiber Reinforced Polymer Composite Cross-arms for Transmission Tower Applications

Vijayvignesh Namasivayam Sukumaar[1] · Mohamad Ridzwan Ishak[1,2,3] · Mohd Na'Im Abdullah[1] · Mohamed Yusoff Mohd Zuhri[3,4] · Muhammad Asyraf Muhammad Rizal[5,6]

Received: 1 April 2025 / Revised: 4 July 2025 / Accepted: 14 July 2025 / Published online: 22 July 2025

Abstract

Pultruded glass fiber-reinforced polymer composite is used for cross-arm constructions. This research focusses on creep response and deflection behavior using cantilever test conditions. The behavior of structurally strengthened cross-arms is evaluated under both short-term and creep scenarios to understand how structural installation affects their performance. By applying Findley's power law, it is ascertained that this empirical method can replicate the cross-arm's viscoelastic response. The outcomes demonstrate the effect of sleeve structures in decreasing the deflection and increasing the resistance to bending forces. Point Y3 exhibited the largest strain according to long-term creep testing, but the reinforced cross-arm showed better resistance. This observation proves that the point Y3 endures the highest stress during operation thereby becomes the point of initial of rupture. Experimental results show an enhancement by the addition of sleeve retrofit under instantaneous and long-term static loading conditions by about 28.50% and 23.50% respectively. Life span prediction showed that both the variants had a notable decline in average elastic modulus over 50-year period, with the upgraded version being about 50% stronger with the corresponding increase in reduction factor by a value of 0.21. As a result, this analysis confirms that the sleeve-retrofitted composite cross-arms possess superior creep capabilities and confine to feasible installations for such applications. The generalized equation for the prediction of the effective utilization of the cross-arm based on the Findley numerical model had been established.

Keywords Sleeve reinforcement · Pultruded glass fiber composite · Creep · Elastic moduli · Cross-arm

✉ Vijayvignesh Namasivayam Sukumaar
n.s.vijayvignesh@gmail.com

✉ Mohamad Ridzwan Ishak
mohdridzwan@upm.edu.my

Mohd Na'Im Abdullah
naimabdullah@upm.edu.my

Mohamed Yusoff Mohd Zuhri
zuhri@upm.edu.my

Muhammad Asyraf Muhammad Rizal
muhammadasyraf.mr@utm.my

[1] Department of Aerospace Engineering, Universiti Putra Malaysia, 43400 UPM Serdang, Selangor, Malaysia

[2] Aerospace Malaysia Research Centre (AMRC), Universiti Putra Malaysia, 43400 UPM Serdang, Selangor, Malaysia

[3] Laboratory of Biocomposite Technology, Institute of Tropical Forestry and Forest Products (INTROP), Universiti Putra Malaysia, 43400 UPM Serdang, Selangor, Malaysia

[4] Advanced Engineering Materials and Composites Research Centre (AEMC), Department of Mechanical and Manufacturing Engineering, Universiti Putra Malaysia, 43400 UPM Serdang, Selangor, Malaysia

[5] Engineering Design Research Group, Faculty of Mechanical Engineeting, Universiti Teknologi Malaysia, 81310 Bahru, Johor, Malaysia

[6] Centre for Advanced Composite Materials (CACM), Universiti Teknologi Malaysia, 81310 Bahru, Johor, Malaysia

1 Introduction

The high-rise electrical transmission towers constitute as the primary functional part of the power system as they act as pillars to uphold conductor lines to transmit power between power plants and substations. Initially, such towers in Malaysia were constructed using latticed steel structures [1, 2]. Figure 1 illustrates various parts of the transmission tower. The most crucial part are the cross-arms whose functionality is to sustain insulators and utility cables at operational heights above the ground level. The cross-arms were then made of wood obtained from Chengal trees due to their capability to resist electrical arcs [3–6]. However, natural wood defects due to tropical environmental conditions and unavailability of structurally graded wood coupled with poor mechanical performance resulted in reduced service life of just 20 years causing disruption in transmission and increased maintenance costs [4, 7].

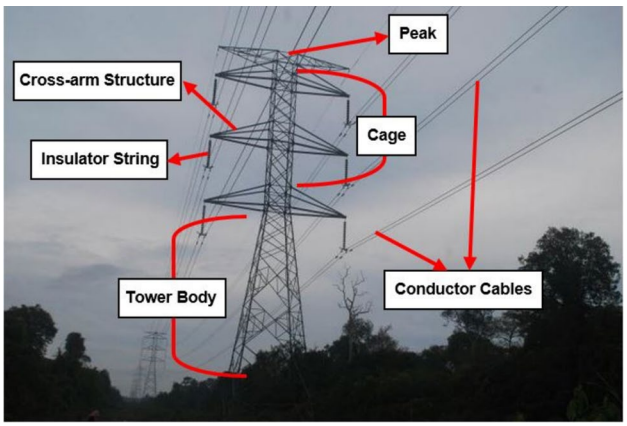

Fig. 1 Parts of an electrical transmission tower

To address these issues, pultruded glass fiber-reinforced polymer (PGFRP) composite has been employed as a material for cross-arms [4, 8]. The highlighted advantages of PGFRP composite are biodegradation resistance, arc quenching, high mechanical rigidity, flexibility in design, and lightweight counterparts, which makes them sought after [9]. The pultrusion technique is employed to manufacture symmetrical square-tubed PGFRP composite cross-arm by utilizing E-glass fibers wetted with unsaturated polyester due to their ease of production and exceptional mechanical properties [10]. The cross-arms possess inherent anisotropic nature and are mechanically strong in the longitudinal direction of fiber orientations. The cross-arm diagrammatic representation is shown in Fig. 2.

There exists an unanticipated failure jeopardizing the structural integrity of transmission towers due to seismic vibrations, dynamic wind loads, constant variation in temperature and humidity, cable snap jerks, and creep failure [1, 9, 11]. This phenomenon of catastrophic failure is problematic as it can lead to fatal accidents to adjacent entities and disruptions in high-voltage electricity supply, which in turn leads to increased repair and maintenance costs [12–15]. Inadequacy in reinforcement wettability and laminate orientations [16, 17], compressive and tensile failures [18] might cause such sudden failures and decreased resistance to material creep failures [19, 20].

In recent years, cross-arm failures have become a significant concern, with no definitive long-term solution currently available. At present, additional structural components

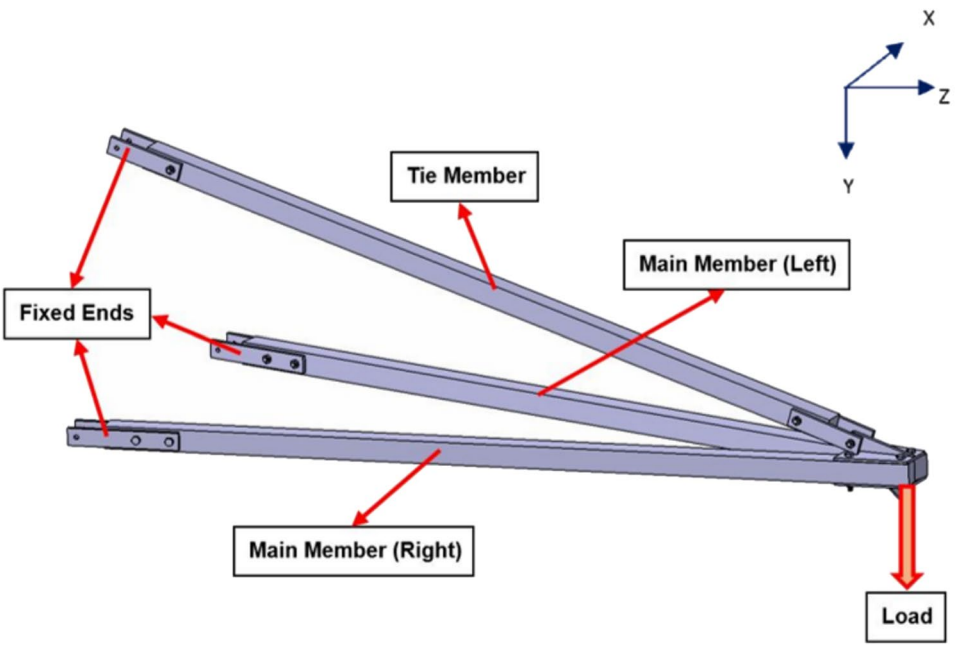

Fig. 2 Parts of an assembled PGFRP composite cross-arm

are often incorporated in an attempt to extend their service life. Previous studies have explored the effects of bracing on cross-arm members [21, 22], and numerical analyses have been conducted to assess the impact of such support systems on various configurations [23, 24]. It is worth noting that transmission tower designs themselves frequently employ bracing elements. However, these reinforcements may introduce additional stresses on the beams, which can lead to issues like slippage. They also come with other disadvantages, such as increased complexity during installation, repair, and maintenance.

Another approach has involved attaching honeycomb sandwich panels to the outer surfaces of PGFRP composite cross-arms [25, 26], typically using polyester resin as an adhesive. However, in tropical climates, these resins are highly vulnerable to environmental degradation: ultraviolet (UV) exposure can lead to surface charring, elevated temperatures can weaken their mechanical properties, and moisture can compromise adhesive strength [27–29]. Given that cross-arms operate under both dynamic loading and harsh environmental conditions, the durability of these honeycomb-reinforced systems is questionable. Furthermore, their implementation demands significant cost, time, and labor, along with frequent maintenance, making them a less sustainable option in the long term.

While PGFRP composite cross-arms have demonstrated superior performance compared to traditional wooden beams, they still encounter notable sustainability challenges. Over time, their mechanical strength deteriorates due to prolonged exposure to environmental factors. The combined effects of mechanical stress from transmission lines and harsh weather conditions contribute significantly to structural degradation. Existing remedial measures, such as temporary bracing and the use of honeycomb panels, serve only as interim solutions. These approaches are not only expensive and labor-intensive but also fail to effectively address the core issue of buckling, which primarily results from the slender geometry of the cross-arm. Furthermore, previous studies that identify failure as occurring at a single point overlook the reality that long, dynamically loaded structures often experience stress distribution over extended regions rather than at isolated points. Therefore, a more comprehensive structural strengthening strategy is necessary, one that not only tackles these shortcomings but also is also practical to implement.

The structural sleeve reinforcement is proposed as a practical and effective alternative, aimed at improving service life by incorporating structural reinforcement. This solution also addresses material availability, manufacturability, installation, and ease of repair, and maintenance. Additionally, this project aims to develop a novel plug-in type insulated sleeve-reinforced composite cross-arm structures with an emphasis on load-bearing capacities and durability of high-rise transmission towers. These initiatives seek to pinpoint the root causes of reported material malfunctions and offer substitutes with increased load capacities and extended service lives.

Sleeve retrofitting is an effective structural enhancement technique that involves encasing a critical segment of a structural member with an external sleeve, typically fabricated from high-strength materials, such as steel, fiber-reinforced polymers (FRPs), or hybrid composites. This method significantly improves the load-bearing capacity and stiffness of the original member by introducing confinement, distributing applied stresses more uniformly, and limiting local deformations. The sleeve acts as a secondary load path, reducing stress concentration in the primary structure and mitigating failure modes, such as buckling, cracking, or delamination. Technically, the retrofit enhances the member's flexural and shear resistance, especially in regions prone to high moment or compressive forces. Moreover, sleeve retrofitting is minimally invasive and can be tailored to the geometry and stress profile of the structure, making it suitable for in situ strengthening under service conditions. Its application is particularly beneficial in structures exposed to dynamic loading or aggressive environmental conditions, where durability and long-term performance are critical.

The effectiveness in handling loading patterns similar to those of cross-arms makes sleeve structures a preferred choice [30, 31]. It was demonstrated that incorporating sleeved panels enhanced the overall mechanical properties, particularly with the increase in fiber infill [32]. Studies have also showed that in comparison to pure nylon, the nylon-reinforced polymeric sleeves, which functions similar to a rubbery medium, exhibited superior dynamic mechanical characteristics and a notable rise in distortion temperature [33]. The sleeves thus hold the potential to provide the sufficient load sustaining capability resisting yielding resulting in rupture under long-term applications. A summary of variety of cross-arm challenges is included in Table 1 along with the proposed solutions examined through investigations.

Notably, PGFRP composite beams behave differently from traditional materials like concrete and steel because of their significant material anisotropy and comparatively low modulus of elasticity [45, 46]. While recent research has concentrated on viscoelastic theoretical modeling composite architectures [47, 48], few data are still available in the literature on the application of PGFRP composite in assembled cross-arm because of the strict limitations on their deformability behavior. A theoretical method was devised for examining both minor and major deflections in a cantilever beam, namely linear transverse deflection and vertical tip deflection respectively [49]. Usually, the Hooke's law and the Bernoulli–Euler theory are used to examine the beam's bending behavior [50–52].

Table 1 Problems faced by cross-arms and their proposed solutions

Cross-arm problems	Proposed solutions	Refs
Corrosion and aging of steel & wooden cross-arms subjected to environment	Adoption of glass fiber-reinforced polymer composite material	[34, 35]
Higher self-weight of cross-arms	Introducing variations in fiber laminate stacking and raster angles	[36, 37]
Reduced durability of cross-arm over longer time period	Incorporation of bracing fixtures encompassing tie and main members	[23, 24, 38]
Redundancy in structural reinforcement and higher slip potential	Install honeycomb structure and filament winding at critical point	[25, 26, 39–42]
Increased slackness of electrical lines due to higher offset of cross-arms	Fasten the cross-arms to body of the tower	[43]
Practical loads and varying environmental conditions deflate the mechanical properties	Utilize hybrid natural fiber or filled-honeycomb sandwich structure reinforced polymer composite	[44]

A mechanical characteristic known as the creep phenomenon happens in materials that are exposed to continuous static stress for extended periods of time. There are multiple phases in the creep process, including primary, secondary, and tertiary deformations, each of which is distinguished by distinct behavior [53, 54]. Studies have indicated that PGFRP composite cross-arms have stronger steady creep characteristics and significantly higher flexural strength than cross-arms made of Balau wood, making them a feasible option as cross-arm material [42, 55]. Nonetheless, it's crucial to understand that there exists a possibility for the PGFRP composite cross-arms to lose mechanical integrity problems and structural shortcomings over time, based on environmental circumstances and the characteristics of the materials.

Furthermore, a number of research have looked into stacking sequences, coupon-scale PGFRP composite cross-arms, creep behavior at varying stress levels, as well as using mathematical models such as the Findley power law [16, 56, 57]. Additionally, studies showed that PGFRP composite cross-arm specimens resulted in brittle failures, when exposed to high temperatures and fluctuating stress levels, in four-point static bending tests with mathematical model validation [58]. In order to fill in these knowledge gaps, this study focusses on full-scale assembly deflection–creep behavior of PGFRP composite cross-arms under real-time operational conditions. The creep testing helps in analyzing and forecasting deflection behavior over the long run.

Furthermore, no experimental research has examined the effects of using a composite structure reinforced with sleeves to enhance the cross-arm. Most existing studies focus on the properties at the coupon scale or solely at the material level. This study presents cross-arm structural analysis methods, complemented by experimental data and an empirical model, to evaluate the deflection behavior of a full-scale sleeve-reinforced PGFRP composite cross-arm.

2 Methodology

The detailed investigations of this study are discussed in the forthcoming sections. Figure 3 illustrates the flowchart of incorporated methodology.

2.1 Materials

A couple of major members and a tie member make up the cross-arm's construction. However, as the main cross-arm part is crucial to the transmission tower's capacity to carry the transmission line, this study only looks at it. The cross-arm features a square cross section of 102×102 mm^2 and a wall thickness of 7.8 mm [4, 9]. The cross-arm main members measure 3651 mm in total length. The inherent properties are summarized in Tables 2 and 3.

The sleeve reinforcement was fabricated using stainless steel (SS) sheets of structural grade 304 with a mill finish standard, specifically SS304-2B, sourced from Tan Central Metal in Selangor, Malaysia. The length of the sleeve reinforcement was kept constant at 1200 mm. This was based on the reported critical failure region of the main cross-arm member, which spans about 1000 mm, as well as Ashby's material section chart, which suggests that reinforcement materials should be more durable than the base material [63].

The thickness of the sleeve was also set as constant measuring 2 mm, that is approximately equal to 1/4th of the wall thickness of the PGFRP composite cross-arm, such that its neither too small where it will not have any or negligible effect (due to improper load transfer, too weak to resist deformation) nor too large wherein it would lead to difficulty in fabrication (due to cold shut/ hot tear, induced self-weight) of the sleeve material.

Since the primary motive is to fabricate a plug-in type reinforcement that can directly be incorporated to the

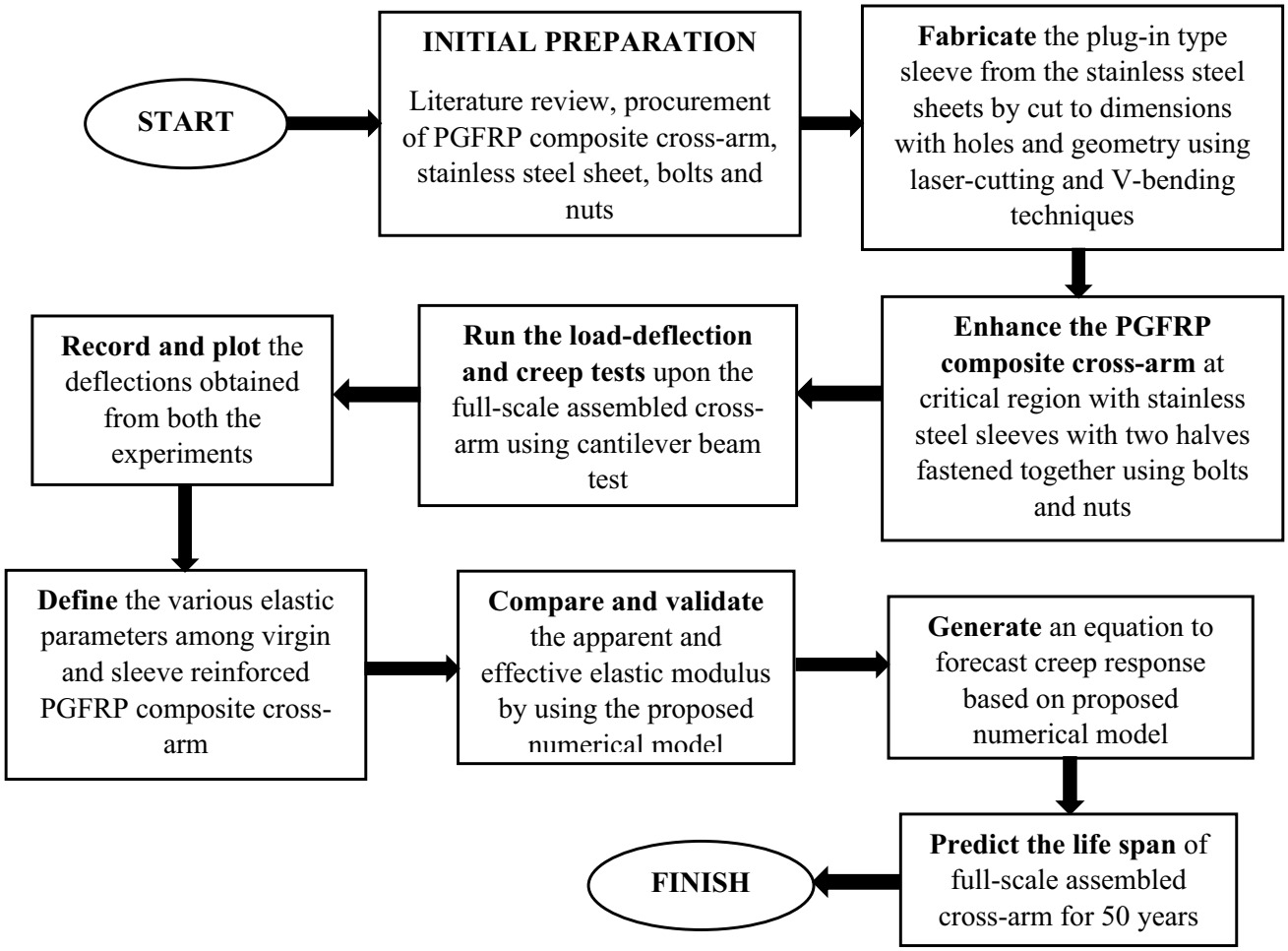

Fig. 3 Flowchart of incorporated research work

Table 2 Properties of PGFRP composite [59, 60]

Property	PGFRP composite
Density	2580 kg/m^3—E-glass 1350 kg/m^3—Unsaturated polyester
Texture	Fine, homogenously and unidirectional fiber along the matrix
Shrinkage	Low
Natural Durability	Low
Modulus of Elasticity	29.8 GPa
Modulus of Rupture	858.0 MPa

Table 3 Parameters of PGFRP composite [61, 62]

Composition		
Material	Resin	Fiber
PGFRP Composite	Unsaturated polyester (UPE) (63 vol. %)	E-glass fiber (37 vol. %)
Parameters		
Composite layer	Orientation (°)	Thickness (mm)
First (Outer)	45	0.5
Second	− 45	0.5
Third	90	0.7
Fourth	0	3.6
Fifth (Inner)	45	0.7

existing cross-arm members without having the need to decouple the assembly, the sleeves were made as two symmetrical halves such that they encompass all the faces of the PGFRP composite cross-arm with flanges, measuring 30 mm with continuous holes upon them of diameter measuring 8 mm with a center distance of 20 mm. The SS304 sheets were transformed into sleeves by laser cutting, laser drilling, and V-bending by Kejuruteraan Tetap Maju, Selangor, Malaysia. The M8 bolts, nuts, flat and spring washers made of SS304 with bolts having a fine thread pitch of 1 mm and a length of 18 mm and bolts with a hexagonal head are obtained from Hua Hui, Zhongshan, China.

Although this study does not focus on the electrical conductivities of materials used, the stainless steel is chosen as they are many folds less conductive than the previously used mild steel and aluminum as reinforcement [21, 22, 25, 26]. Additionally, the interface between PGFRP composite cross-arm and sleeve is insulated using the silicone rubber sheets, with thickness measuring 1.5 mm, obtained from HardwareMISE Sendirian Berhad, Johor, Malaysia which provides additional roles as a water-proof medium and in reducing slip potential. Figure 4 illustrates the primary step involved in fabrication of sleeve.

The second phase of the specimen preparation installs the sleeve to the cross-arm main members. In order to improve adhesive strength and guarantee a long-lasting bond, the silicone rubber, which was added to create a cushioning effect, is glued to the cross-arm's surface using epoxy resin and a quick-setting hardener in a 40:1 by weight ratio [64, 65]. This was acquired from Hardex Corporation Sendirian Berhad, Pahang, Malaysia. The two halves of the sleeve are symmetrically positioned, ensuring a transition fit at the mid-point of the cross-arm. This location is considered the most critical region for failure as the mid-point experiences the peak stress under loading [22, 26].

These two halves are fastened together using the bolts, nuts, and fasteners in the arrangement of bolt—flat washer (top face)—spring washer (bottom face)—nut, to ensure maximum strength of fastening as flat washers distribute the fastener's load and the spring washers counters vibrations [66, 67]. The fine-threaded bolt due to their large contact area ensures the higher strength of reinforcement in tension and shear [68]. Prior to this, the cross-arm's surface was dedicatedly prepped by wiping off any dust using a smooth cloth and sandpaper. The transition fit sleeve-mounted PGFRP composite cross-arm and other prominent materials used are illustrated in Fig. 5, which is immediately ready to be subjected to characterization unlike the previous technique [25, 26].

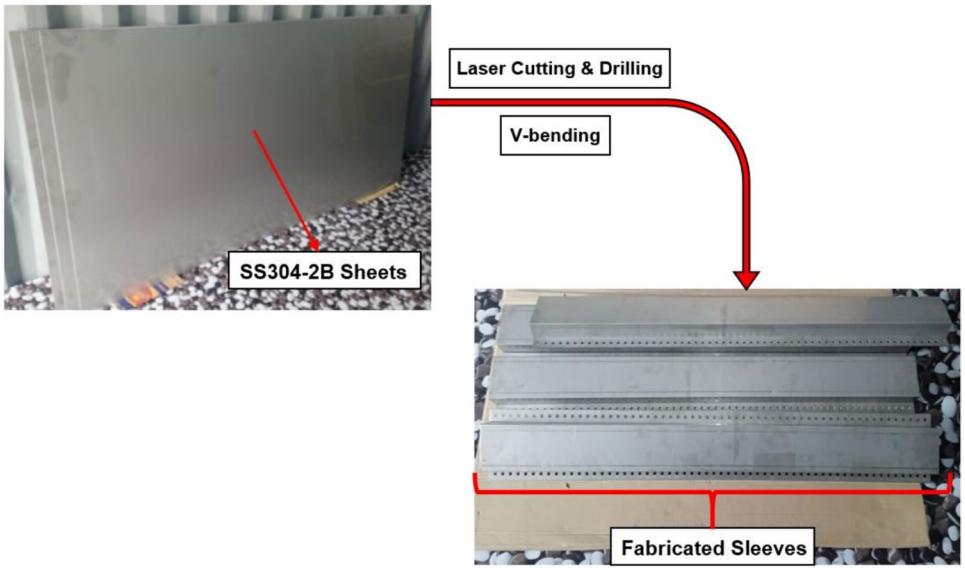

Fig. 4 Fabrication of sleeve from base material

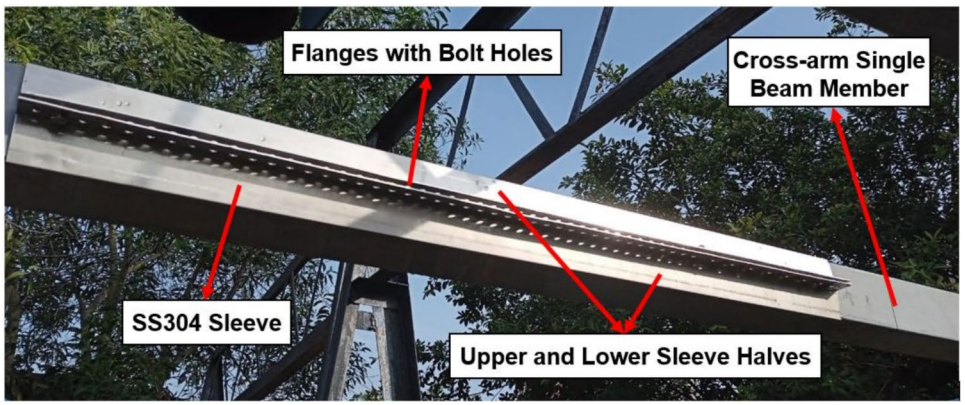

Fig. 5 Transition fit mounted sleeve

2.2 Experimental Setup

In this work, full-scale assembly cross-arm conditions were used for testing. The previous work of cross-arm test design served as the foundation for the testing procedure development [69]. The suspended loads induced movement along the longitudinal axis, which were measured using Mitutoyo 2050A analog dial gages from Japan. At the hangar facility in the Engineering Faculty of Universiti Putra Malaysia, the test was carried out in a tropical environment.

The strain gages could potentially detach or become misaligned under heavy load application, which may affect the accuracy of the results. Given that the most significant failure occurs along the cross-arm's Y-axis, the deflection measurements were limited to this direction [12, 70]. Along the main members, the gage spacing was determined to be 0.61 m. This dial gage configuration followed the research technique described in earlier studies [69, 71]. Figure 6 indicates the measurement gage positions formulated as per previous studies [23, 26].

2.2.1 Load–Deflection Test

Two primary main members and one tie member constitute an assembled cross-arm. After assembly, the cross-arms were lifted to the appropriate height using a forklift, following the necessary setup and fitting adjustments. The final position of the cross-arms was carefully fine-tuned using the forklift to ensure precise alignment with the gearbox tower's position. Figure 7 illustrates the cross-arm assembly on the test rig. For the load–deflection test, a concrete block weighing approximately 1.6 tons was used as the applied load [25].

2.2.2 Creep Test

The dial gage setup and cross-arm positions were identical to those shown in Fig. 6. As illustrated in Fig. 8, a load was suspended from the free end of the cross-arm. Following the ASTM D2990 standard, a creep test was carried out for 1000 h. During this period, deflection values were recorded at intervals of 0, 0.1, 0.2, 0.5, 1, 2, 5, 20, 50, 100, 200, 500, 700, and 1000 h. First strain (also known as "immediate strain") was measured 15 s after the working tension was applied. Real-time exposure to tropical weather and environmental factors was used to simulate real-world operational circumstances for the cross-arms.

2.3 Numerical analysis

The load induced is directly proportional to the deflection produced. It is negligible in contrast to its yielding characteristics [72]. According to Hooke's law, force is proportional to extension produced when a constant load is induced [73]. Therefore, Eq. (1) can be used to determine the stress–strain relationship of the cross-arm which is visually represented in Fig. 9.

$$P = k\delta \tag{1}$$

where P represents the force (N), k denotes the elastic coefficient (N/m), and δ signifies the deflection (m).

The moment of inertia for the square cross section is incorporated into Eq. (1), resulting in the following expression:

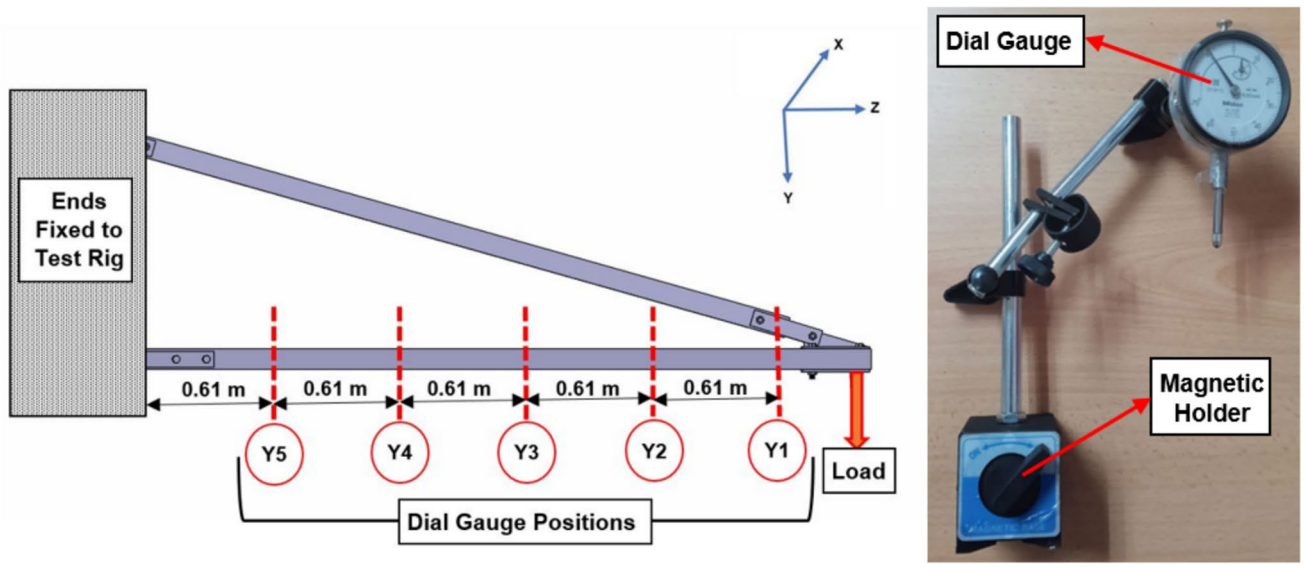

Fig. 6 Position of dial gages upon the cross-arm and assembled dial gage setup

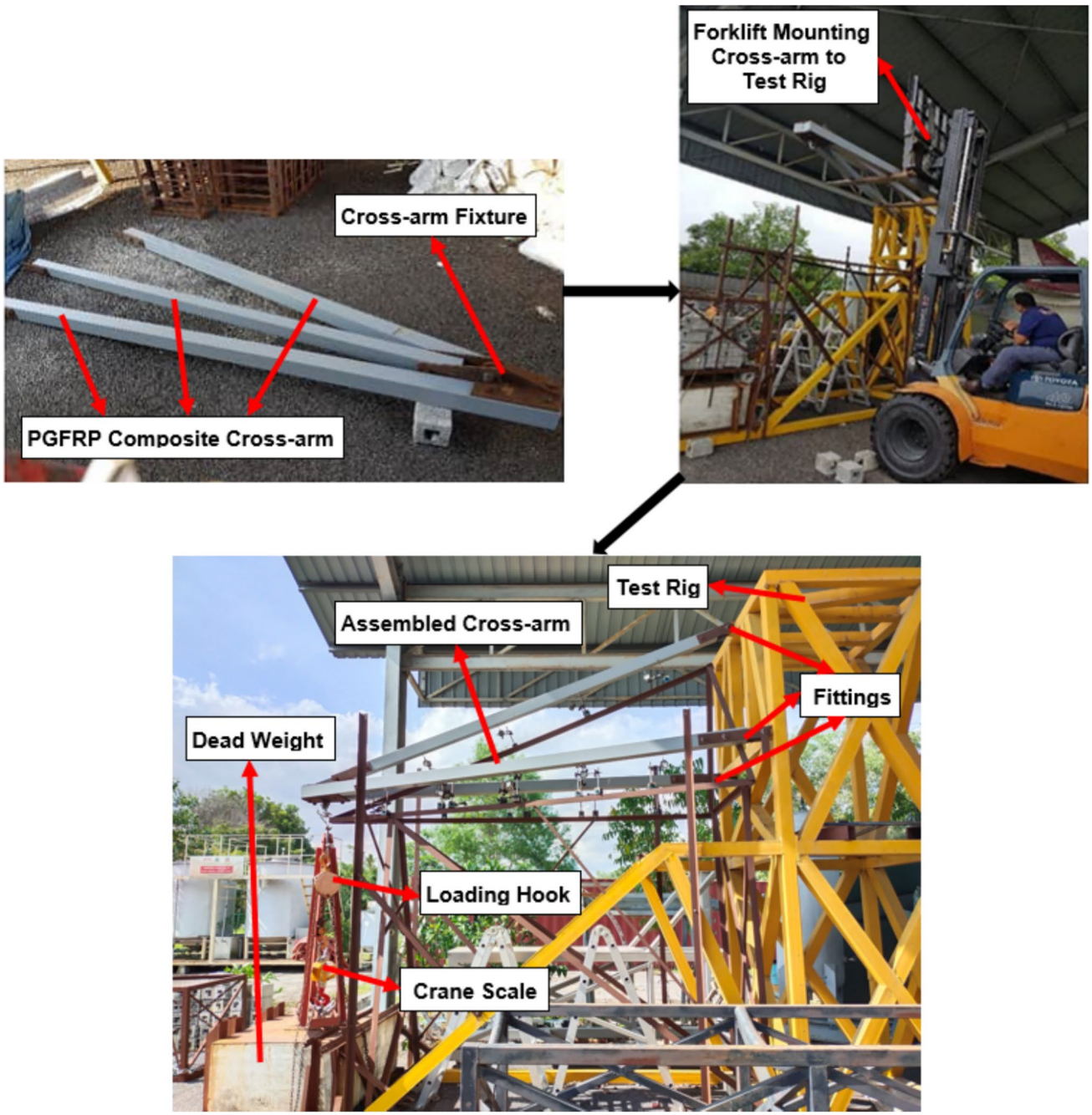

Fig. 7 Assembly cross-arm mounting upon the test rig

$$E_e = \frac{4PL^3}{\delta bh^3} \tag{2}$$

where E_e represents the elastic modulus (GPa), L denotes the length of the beam (m), b signifies the breadth of the beam (m), and h mentions the thickness of the beam (m). Additionally, other parameters, according to Hooke's law, can be expressed as shown in Eq. (3) and Eq. (4) [53, 74].

$$\sigma = \frac{P(L-x)\frac{h}{2}}{I} = \frac{6P(L-x)}{bh^2} \tag{3}$$

$$\varepsilon = \frac{\sigma}{E_e} \tag{4}$$

Fig. 8 Creep test setup

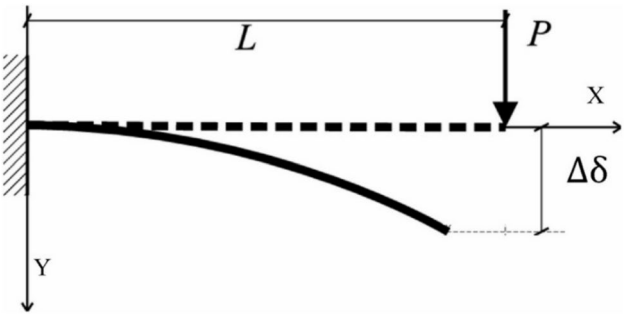

Fig. 9 Cantilever beam concept

From the above equations, it is evident that the maximum stress occurs at the fixed ends (x = 0), while the lowest stress is observed at the free ends (x = L).

The long-term resilience of a material is expressed in terms of strain per unit stress using a measurement known as creep compliance. It can be understood as a mathematical equation that can be found with the help of Eq. (5).

$$J(t) = \epsilon(t)/\sigma_0 \tag{5}$$

where σ_0 represents the initial stress applied in MPa, $\epsilon(t)$ denotes the strain that changes over time, and $J(t)$ indicates the creep compliance in MPa^{-1}.

2.4 Empirical Numerical Model

The Findley power law model was applied to describe the time-dependent strain behavior of the sleeve-retrofitted PGFRP cross-arms. This model is widely used in polymer composite creep studies due to its simplicity and accuracy in predicting viscoelastic deformation. In terms of stress and material constants, this model clarifies transient creep. Being widely applicable, its numerical computation is straightforward. The elastic strain (ε) was substituted with the applied stress (σ) and then divided by the modulus of elasticity (E), resulting in Eq. (7) as follows:

$$\varepsilon(t) = \varepsilon_0 + mt^n \tag{6}$$

$$\varepsilon(t) = \frac{\sigma}{E} + mt^n \tag{7}$$

where $\varepsilon(t)$ represents strain as a function of time, ϵ_0 represents instantaneous strain, t represents time (h), m represents load constant and n represents material constant obtained from non-linear curve fitting of experimental data. For the elastic modulus defined as a function of time, its reduction factor $\varphi(t)$ is defined in Eq. (8) and Eq. (9).

$$\varphi(t) = \left(1 + \frac{E_0}{E_t} * t^n\right)^{-1} \tag{8}$$

$$E_a(t) = E_0 * \varphi(t) \tag{9}$$

where E_0 represents initial elastic modulus (GPa), E_t represents elastic modulus at a specific time (GPa), and $E_a(t)$ represents apparent elastic modulus subjected to creep. Hence, the forecasting of the behavior of full-scale cross-arm can be done by incorporating Eq. (7) in Eq. (8) thereby generating Eq. (10).

$$E_a(t) = E_0 * \left(1 + \frac{E_0}{E_t} * t^n\right)^{-1} \tag{10}$$

3 Results and Discussion

3.1 Load–Deflection Response

A comparative study involved two types of PGFRP composite cross-arms, namely without (virgin) and with sleeve reinforcement. The applied stress was 1.5 times the usual induced load, reaching 9705 N [25]. The deflection behavior is illustrated in Fig. 10 shows precise proportionality and consistent with other research. This relationship held true as long as there was minimal variation and the beam material

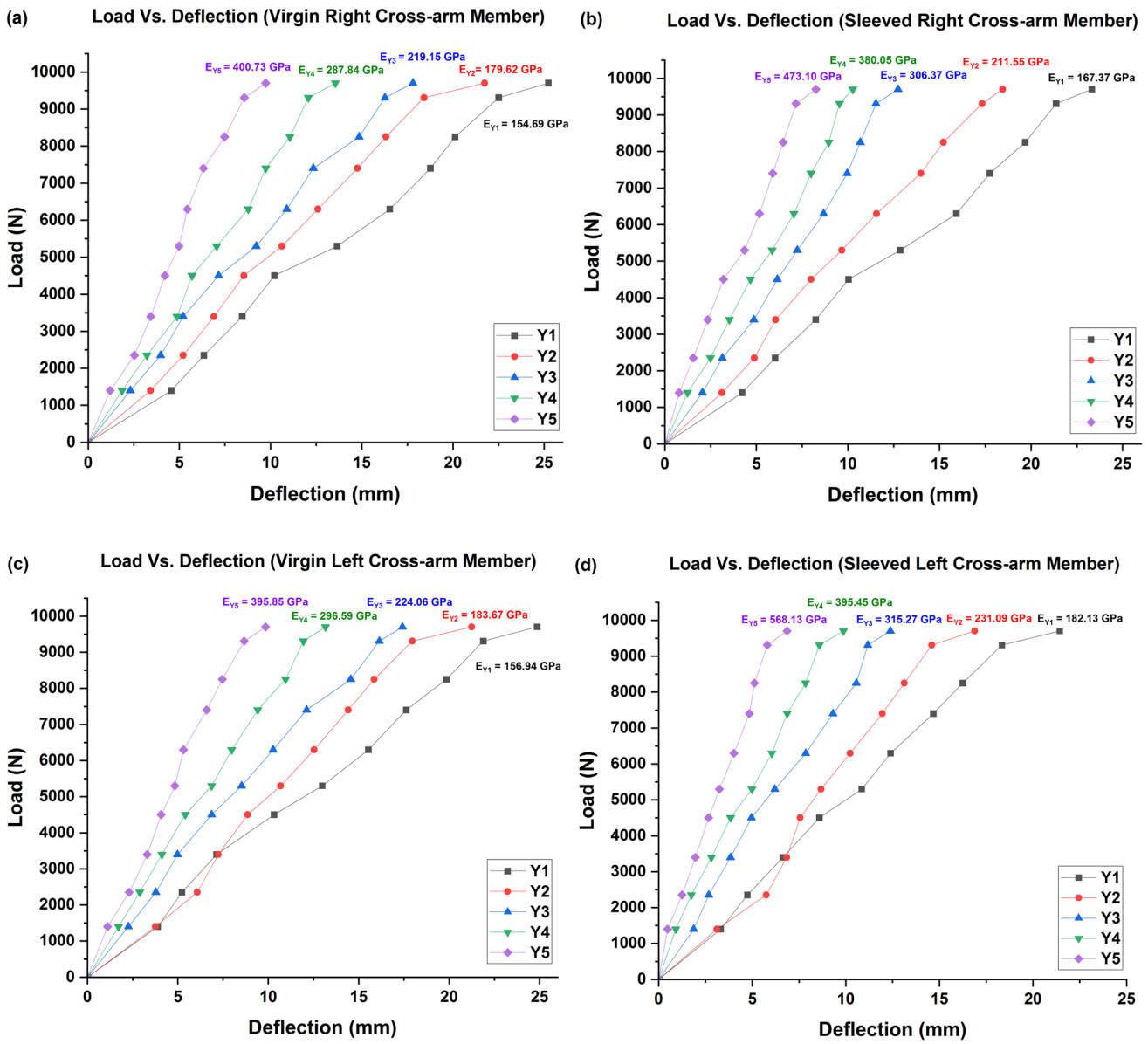

Fig. 10 Load deflection plots of PGFRP composite cross-arm upon (**a**) virgin right main member (**b**) sleeved right main member (**c**) virgin left main member (**d**) sleeved left main member

did not experience yielding [75, 76]. Since the beam's length was greater in comparison to thickness and deformation curvature radius, Poisson's ratio had no significant effect [77]. The mid-point Y3 on the cross-arm main member is also referred to as the peak stress point as reported by previous research. It can be observed that there exists a minuscule difference in deflection values obtained between the right and left cross-arm main members that could be attributed to minor structural deviations from assembly test rig fittings. Furthermore, as shown in Fig. 10, a gradual decrease in deflection values is observed from points Y1 to Y5.

However, the reinforcement along the critical stress region for the sleeve-reinforced PGFRP composite cross-arm is notably lower compared to the virgin cross-arm due to the reinforcement along its critical stress region. This is because the virgin cross-arm has been modified by the incorporation of sleeve to include a high-quality bending behavior, thereby resisting deflections under induced loads. The combination of the PGFRP composite cross-arm and sleeve construction collectively boosts durability, resilience, and structural integrity [78].

It can be observed that sleeve-reinforced PGFRP composite cross-arm shows reduced deformations values all the dial gage positions especially at the peak stress point Y3. At point Y3, the right main member's deflection value decreased from 17.81 to 12.74 mm, while the

left main member's deflection value decreased from 17.42 to 12.38 mm thereby showing a decrease in deflection by 28.46% and 28.93% respectively, which are much higher than the previous research upon incorporation of honeycomb sandwich structure [25]. Additionally, the installation of a plug-in type insulated sleeve structure possessing higher durability and stress transfer capability can be attributed to delayed yielding of the cross-arm and increasing the rigidity and toughness of the material.

Since the reinforced PGFRP composite cross-arm's elastic modulus exhibits higher values at all specified places than the virgin cross-arm, the virgin cross-arm's strength will be lower [71]. However, the points Y4 and Y5 resulted in a reduction of elastic modulus [25]. This could be due to the reinforced area of the cross-arm absorbing more of the load, which leads to a lower elastic modulus value at the point after the structure was enhanced [79, 80].

This issue has been successfully resolved by implementation of the current proposed research solution. The peak stress at point Y3 increased from 219.15 to 306.37 GPa for the right cross-arm main member, and from 224.06 to 315.27 GPa for the left cross-arm main member. Along with these improvements, the overall strength and elastic modulus of the cross-arm structure have increased as anticipated when reinforcement (sleeve) is applied [81].

3.2 Creep Response

The testing protocols adhered to the previously set standards [22, 69]. The static load was set at 6467 N. This standard also defined the vertical force exerted on the constructed cross-arm under operating conditions [69]. As shown in Fig. 11, the testing duration, in accordance with ASTM D2990 standards with an average ambient temperature of 29.3 °C and a relative humidity of 70.38%.

Relative humidity (RH) significantly affects the creep behavior of polymer matrix composites due to the hygroscopic nature of the matrix materials. Moisture absorbed under high RH conditions acts as a plasticizer, disrupting intermolecular forces that leads to a reduction in stiffness, elastic modulus, and glass transition temperature (Tg) increasing time-dependent deformation under sustained loads [82]. Water molecules can weaken interfacial adhesion through physical and chemical mechanisms, leading to debonding, microcracking, and reduced structural integrity. As a result, composites under high RH conditions exhibit accelerated creep due to compromised stress distribution across the composite system. Additionally, moisture absorption causes differential swelling between the fibers and the matrix. This mismatch generates internal stresses and localized damage, further contributing to creep [83]. The effect is more pronounced when elevated RH is coupled with high temperatures as moisture diffusion increases and the

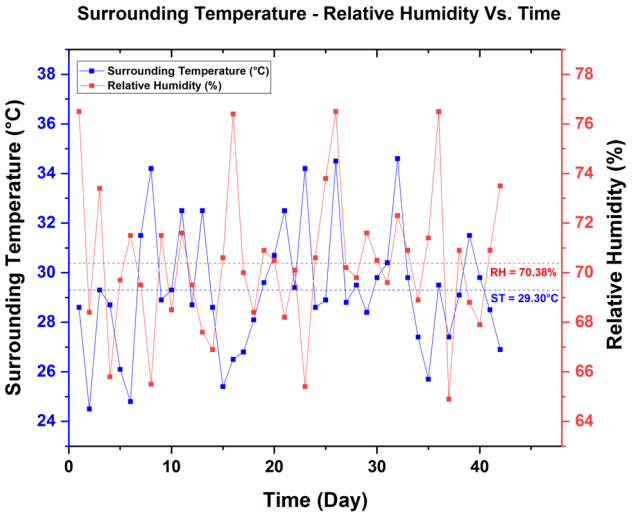

Fig. 11 Recorded temperature and relative humidity for creep test

matrix softens further, amplifying viscoelastic and viscoplastic deformation. Empirical studies show that composites exposed to RH levels above 60% may experience 20–50% higher creep strain compared to those in dry environments [84].

Figure 12 shows the creep strain curves. As the duration of loading increased, the elastic strain was found to change upon the cross-arms [85]. This investigation found the highest creep strain at the mid-point, point Y3 [25, 71]. This observation showed that the cantilever loading induced varying deflections subjected to the distance between the load and measured points [86, 87].

This outcome is significant since it demonstrates the cross-arm's ability to tolerate and sustain the loading circumstances [88]. Compared to earlier studies, it was found that plug-in type sleeve reinforcement could significantly improve the assembly cross-arm structure's structural integrity and creep resistance [25, 39]. Overall, the use of insulated sleeve reinforcement enhanced load-bearing durability and reduced the resulting deformation, thanks to the induced fabric interlayer contact mechanism [89].

The red arrows indicate a prolonged transition period. The addition of the plug-in type sleeve reinforcement structure effectively lowered the viscoelastic stage and increased stability, lowering the likelihood of the structure collapse. The strain value at point Y3 was higher than the values at the other points (Y1, Y2, Y4, and Y5) along both the left and right cross-arm members. This observation yet again ascertains that the mid-point Y3 is the point of failure initiation and hence reducing the stress at that point is primarily more important which has been achieved by the utilization of sleeve reinforcement.

As seen in Fig. 12, the creep strain values at point Y3 on both the right and left virgin cross-arm members exceeded

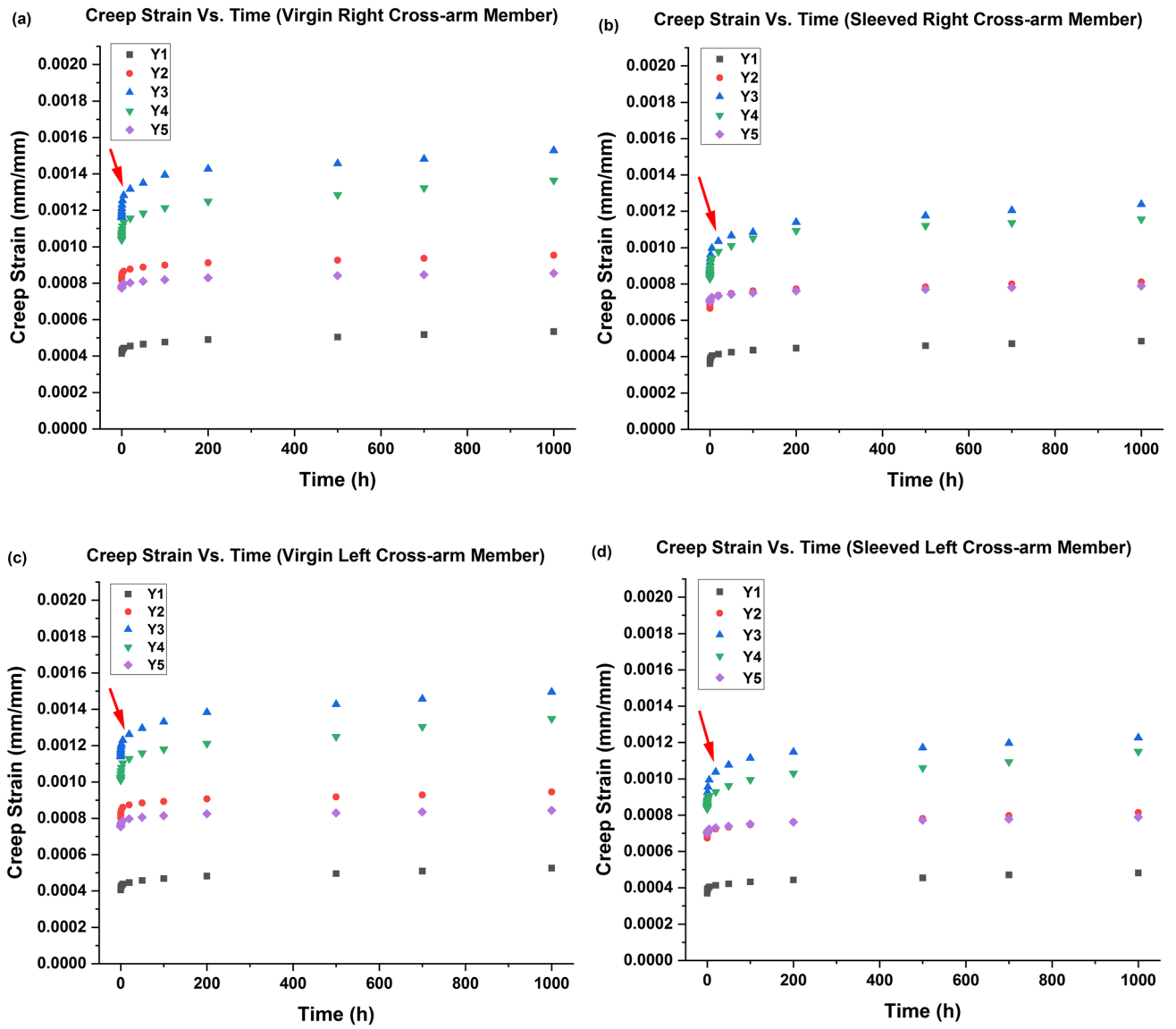

Fig. 12 Creep strain rate plots of PGFRP composite cross-arm upon (**a**) virgin right main member (**b**) sleeved right main member (**c**) virgin left main member (**d**) sleeved left main member

0.0014 mm/mm. In contrast, the values for both the right and left sleeve-reinforced cross-arm members were significantly lower, around 0.0012 mm/mm. Furthermore, the reduction percentages of creep strain in sleeve-reinforced cross-arm members are summarized in Table 4 that shows an overall better result, especially at the peak stress point Y3, than the previous research solution [25].

Table 5 shows the initial and derived experimental parameters with linear proportionality from free to fixed end [90]. The point nearest to the fixed end (Y5) shows the greatest modulus, while the point Y1 exhibits the least. The final values, presented in Table 4, can be attributed to the sleeve installation, which strengthens the structure and stabilizes the creep strain. Overall, it can also be concluded from observation that the lateral deflections induced upon the cross-arms due to the subjected load could also be reduced as the sleeve encapsulates the region under stress and is however beyond the scope of this study as they are minor negligible deflections as slenderness ratio for the current cross-arm structure is less than 200 [57, 91].

Equation (3) was used to calculate the stress at various points along the cross-arm, with the distances measured from the fixed end to the designated points. The dial gages were placed at an equal distance of 0.61 m from the fixed end, resulting in distances of 3.05 m, 2.44 m, 1.83 m, 1.22 m, and 0.61 m. The corresponding stresses were 97.29 MPa, 196.04 MPa, 294.79 MPa, 393.54 MPa, and 492.29 MPa for points Y1, Y2, Y3, Y4, and Y5, respectively.

Table 4 Creep strain values of virgin and sleeve-reinforced cross-arm members

Cross-arm	Creep strain at the end of the testing period (mm/mm)				
	Y1	Y2	Y3	Y4	Y5
Virgin (Right)	0.000534	0.000953	0.001528	0.001364	0.000855
Sleeved (Right)	0.000485	0.000811	0.001238	0.001156	0.000789
Reduction (%)	10.10	17.51	23.42	17.99	8.37
Virgin (Left)	0.000526	0.000945	0.001495	0.001348	0.000844
Sleeved (Left)	0.000482	0.000813	0.001227	0.001150	0.000789
Reduction (%)	9.07	16.27	21.84	17.22	6.97

Table 5 Initial experimental parameters for virgin and sleeved cross-arm members

Cross-arm	Location	σ_0 (MPa)	ε_0 ($\times 10^{-4}$)	$E_{c,0}$ (GPa)
Virgin (Right)	Y1	97.29	4.1359	235.23
	Y2	196.04	8.1622	240.18
	Y3	294.79	11.6133	253.84
	Y4	393.54	10.3807	379.11
	Y5	492.29	7.7239	637.36
Sleeved (Right)	Y1	97.29	3.6156	268.89
	Y2	196.04	6.6557	294.54
	Y3	294.79	8.7099	338.45
	Y4	393.54	8.2991	474.19
	Y5	492.29	7.0118	702.09
Virgin (Left)	Y1	97.29	4.0537	239.93
	Y2	196.04	8.0252	244.28
	Y3	294.79	11.3941	258.72
	Y4	393.54	10.1068	389.38
	Y5	492.29	7.5322	653.58
Sleeved (Left)	Y1	97.29	3.6976	263.12
	Y2	196.04	6.7379	290.95
	Y3	294.79	8.6826	339.52
	Y4	393.54	8.3539	471.09
	Y5	492.29	6.9844	704.84

In essence, Hooke's law indicates that ε_0 for both the virgin and sleeve-reinforced cross-arms is primarily corresponded to the applied load. It was found that the sleeve reinforcement enhanced the durability [92]. The data also show that point Y3 experienced the highest creep strain, and the sleeve reinforcement significantly improved its performance, effectively delaying both crack initiation and crack propagation.

Figure 13 shows the time-dependent compliance graphs determined using Eq. (5) for the PGFRP composite cross-arms that are both virgin and have sleeves. The desired outcome was attained when the data showed that the PGFRP composite cross-arm members with sleeves exhibited significantly lower creep compliance than the virgin PGFRP composite cross-arm respective members.

As they were endured to constantly changing tropical environment throughout the day, the structural deterioration in the virgin PGFRP composite could be responsible for the increase in creep compliance [93, 94]. Fiber pull-off could result from the higher stress magnitude causing microcracks to spread between the fibers [95]. Since the sleeved PGFRP composite cross-arms had a greater bending strength than their virgin equivalent, there was less primary creep. Structurally enhanced PGFRP composite cross-arms have shown the ability to reduce the steady-state creep rate, thereby extending the material's service life while maintaining a consistent load.

3.3 Findley Power Law Creep Model

The Findley power law empirical model, a widely used creep model in cross-arm performance studies, was applied to analyze the creep properties [96]. Using the data from Fig. 12, this model was applied to fit a long-term behavior in order to predict strain at specific time intervals, as shown in Table 6. This process involves fitting curves to determine the parameters specific to each material, *m* and *n*. The equation appears to match the data closely, suggesting that Findley's power law is an effective model for the creep behavior of the PGFRP composite cross-arm. The adjusted R^2 score, which indicates how well the model explains the experimental data, ranged from 0.9696 to 0.9972, values very close to 1 and significantly better than those reported in previous research [25].

It is evident that the structural modification exhibited enhanced transient creep due to observed steady-state creep response. This suggests that the sleeve structure enhances the viscoelastic stage of creep [20, 97]. The transient creep values for the cross-arm's sleeve right member and its virgin counterpart were 44.7330×10^{-6} and 54.7084×10^{-6} respectively and that for the sleeved left member and its virgin counterpart were 23.9100×10^{-6} and 41.2141×10^{-6} respectively. This transient creep strain represents the initial phase of inelastic flow, which gradually decreases until the steady-state period is achieved [98]. However, the *n* values for the upgraded and current cross-arms fell within the typical range for material exponents that are independent of stress [90, 99, 100].

Furthermore, it appears that the *n* parameter is temperature-sensitive, which may be explained by the fact that the test temperatures were close to the glass transition temperature [97]. From the improved load–defection, steady-state creep and transient creep results, it can be confirmed that the

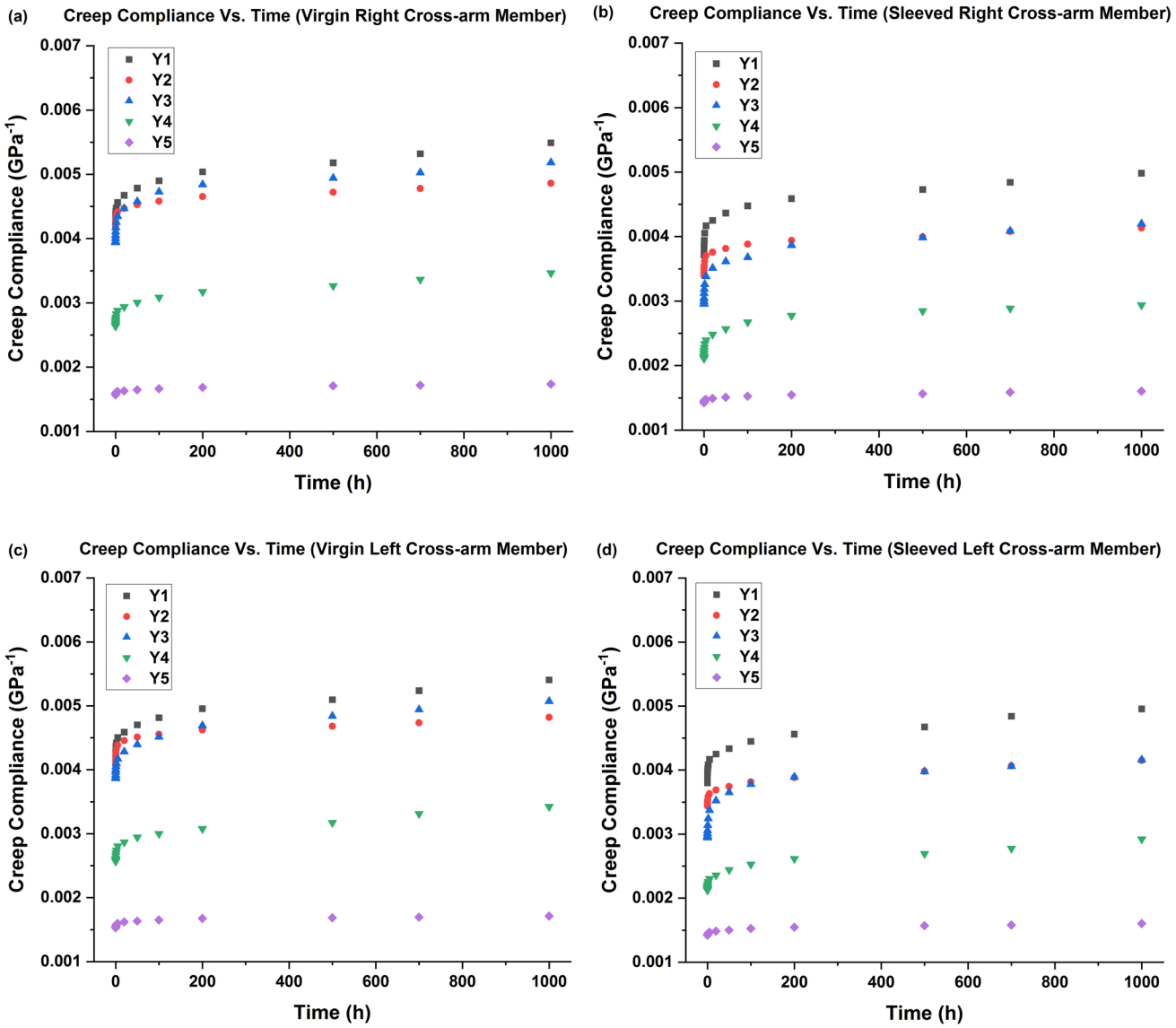

Fig. 13 Creep compliance rate plots of PGFRP composite cross-arm upon (**a**) virgin right main member (**b**) sleeved right main member (**c**) virgin left main member (**d**) sleeved left main member

utilization sleeve structures have ensured compatibility with the PGFRP composite cross-arms for the intended applications in additions to other real-time advantages.

3.4 Creep Model Validation

The initial modulus of elasticity, denoted as $E_{e,0}$, was found to be inversely proportional to the measured points along the cross-arm members. The lowest elastic modulus was observed at the loaded end point, Y1, while the highest was at the fixed point, Y5. Table 7 summarizes this comparison, where the empirical Findley's model was compared with experimental data to determine the initial elastic modulus values. Remarkably, the values obtained were nearly identical, suggesting that the creep behavior of the PGFRP composite cross-arm was well captured by Findley's power law model. Although the assembly cross-arm condition showed a higher value, the results for the elastic modulus under both individual cross-arm and assembly conditions followed the same trend.

Every recorded percentage mistake was less than 5% as shown in Table 7. This indicates that the experimental data and the numerical model (Findley's power law) were in close alignment. When comparing experimental results to numerical values, the acceptable threshold for percentage error is typically considered to be less than 20%. The presented experimental data closely aligned with the numerical model and adhered to the guidelines established by the accurate

Table 6 Summary of parameters obtained and derived from Findley Power Law Model

Cross-arm	Location	ε_0 (10^{-4})	m (10^{-6})	n	$E_{e,0}=\sigma/\varepsilon_0$ (GPa)	$E_t=\sigma/m$ (GPa)	R^2
Virgin (Right)	Y1	4.0934	30.3377	0.2098	237.67	3206.90	0.9811
	Y2	8.0817	43.2536	0.1869	242.57	4532.34	0.9714
	Y3	11.4000	91.5790	0.2094	258.58	3218.97	0.9876
	Y4	10.3000	90.7517	0.1998	382.07	4336.45	0.9858
	Y5	7.6867	17.6200	0.2373	640.44	27,939.27	0.9919
	Average		54.7084	0.2086	352.27	8646.79	0.9836
Sleeved (Right)	Y1	3.5361	20.1716	0.2589	275.13	4823.12	0.9929
	Y2	6.5417	36.2013	0.1973	299.67	5415.28	0.9793
	Y3	8.4958	91.3475	0.2069	346.98	3259.97	0.9881
	Y4	8.0905	58.9801	0.2441	486.42	6672.42	0.9931
	Y5	6.9716	16.9647	0.2348	706.14	29,018.49	0.9925
	Average		44.7330	0.2284	422.87	9837.86	0.9892
Virgin (Left)	Y1	4.0123	20.9641	0.2526	242.47	4640.79	0.9903
	Y2	7.9147	42.8053	0.1832	247.69	4579.81	0.9696
	Y3	11.3000	61.6033	0.2563	260.87	4785.29	0.9972
	Y4	10.0000	54.3924	0.2591	393.54	7235.20	0.9863
	Y5	7.4558	26.3056	0.1936	660.27	18,714.27	0.9757
	Average		41.2141	0.2290	360.97	7991.07	0.9838
Sleeved (Left)	Y1	3.6536	23.7772	0.2258	266.26	4091.73	0.9862
	Y2	6.6908	24.4204	0.2530	292.99	8027.71	0.9916
	Y3	8.3677	10.1579	0.1989	352.29	29,020.76	0.9738
	Y4	8.3054	43.2908	0.2813	473.83	9090.62	0.9914
	Y5	6.9280	17.9042	0.2432	710.58	27,495.78	0.9889
	Average		23.9100	0.2410	419.19	15,545.32	0.9864

Table 7 Comparison of initial elastic modulus between experimental and Findley model

Cross-arm	Initial Elastic Modulus, $E_{e,0}$ (GPa)				
	Location				
	Y1	Y2	Y3	Y4	Y5
Experimental (Virgin Right)	235.23	240.18	253.84	379.11	637.36
Findley Model (Virgin Right)	237.67	242.57	258.58	382.07	640.44
Error (%)	1.03	0.99	1.86	0.74	0.48
Experimental (Sleeved Right)	268.89	294.54	338.45	474.19	702.09
Findley Model (Sleeved Right)	275.13	299.67	346.98	486.42	706.14
Error (%)	2.32	1.74	2.52	2.57	0.57
Experimental (Virgin Left)	239.93	244.28	258.72	389.38	653.58
Findley Model (Virgin Left)	242.47	247.69	260.87	393.54	660.27
Error (%)	1.05	1.39	0.83	1.06	1.02
Experimental (Sleeved Left)	263.12	290.95	339.52	471.09	704.84
Findley Model (Sleeved Left)	266.26	292.99	352.29	473.83	710.58
Error (%)	1.19	0.70	3.76	0.58	0.81

Table 8 Prediction of elastic moduli of assembly structure based on Findley power law

Cross-arm	Equation to predict elastic moduli for the overall assembly cross-arm structure at a given time
Virgin (Right)	$E_{e,virgin(right)}(t) = 258.58 \times \left(1 + \left(\frac{t^{0.2094}}{12.45}\right)\right)^{-1}$
Sleeved (Right)	$E_{e,sleeved(right)}(t) = 346.98 \times \left(1 + \left(\frac{t^{0.2069}}{9.39}\right)\right)^{-1}$
Virgin (Left)	$E_{e,virgin(left)}(t) = 260.87 \times \left(1 + \left(\frac{t^{0.2563}}{18.34}\right)\right)^{-1}$
Sleeved (Left)	$E_{e,sleeved(left)}(t) = 352.29 \times \left(1 + \left(\frac{t^{0.1989}}{82.38}\right)\right)^{-1}$

numerical model, with the percentage error remaining below 20% [101–103]. The present and upgraded PGFRP composite cross-arm's creep characteristics were effectively confirmed by this study using accurate and reliable results.

3.5 Performance Prediction of Assembly Cross-arm

The Findley's equation was applied to predict the elastic modulus over time, $E_{e,virgin}(t)$ and $E_{e,sleeved}(t)$, as shown in Table 8. Point Y3 was identified as the peak stress point, where crack initiation begins, making it a critical point

for forecasting the expected elastic modulus. The reduction factors of the modulus over time ($\chi_{e,virgin}(t)$ and $\chi_{e,sleeved}(t)$) were analyzed. Since the elastic modulus values of the right and left cross-arm members were nearly identical, the average value from both was used to represent the cross-arm curves for both the virgin and sleeved cross-arm components.

Referring to Fig. 14, the early stage, or roughly 24 h into the initial test period, had the greatest stiffness reduction. However, after the early stage phase, the creep rate reduction fell at a slower pace owing to bending. Furthermore, the graph indicates that for both the sleeved and virgin cross-arms, the apparent reduction factor dropped nearly steadily. It was decided to anticipate the reduction factor and effective moduli for the next 50 years.

Upon completion of the experiential period, the average elastic modulus of the virgin cross-arm was 195.20 GPa, reflecting a decrease of about 25% from the original effective modulus. In comparison, the sleeved cross-arm's average elastic modulus dropped by approximately 16%, reaching an effective value of 288.18 GPa. Projections indicate that, after 50 years, the anticipated modulus of elasticity for the virgin cross-arm will be roughly 59% lower than the initial modulus, while the sleeved assembly will experience a 37% reduction. This analysis shows that the use of a plug-in type sleeve structure enhanced the PGFRP composite cross-arm by just over 20%. Variations in the load application method and assembly conditions led to minor differences from the values under individual conditions. However, the overall trend closely mirrored that of the individual cross-arm members.

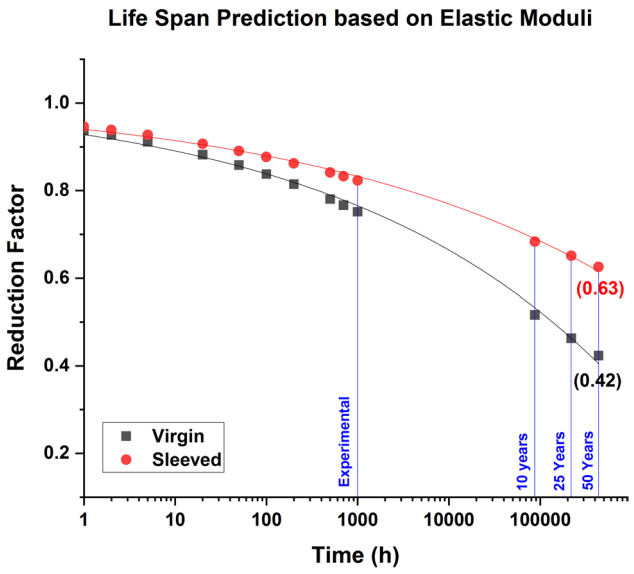

Fig. 14 Life span prediction of cross-arms based on elastic moduli

As shown in Table 9, the predicted elastic moduli for the sleeved cross-arm at 10, 25, and 50 years were consistently higher than those of the virgin cross-arm and significantly outperformed the results from previous research [25]. However, with values close to 0.99, the regression analysis (or curve fitting) for both the virgin and sleeved cross-arms provided the most accurate alignment between the actual and predicted data points [104, 105].

This study shows that the virgin PGFRP composite cross-arm assembly can be reinforced and its lifespan extended by adding sleeve reinforcement to the cross-arms. The maintenance costs of the cross-arm can be reduced as the sleeve can be installed onto existing transmission towers with ease, thanks to the availability of materials, manufacturing methods, and straightforward installation. This approach helps extend the overall lifespan of the assembly.

4 Conclusions

In conclusion, a comprehensive analysis of the operational characteristics of the full-scale PGFRP composite cross-arm assembly in a 132 kV 13 L transmission tower, reinforced with sleeves, has yielded valuable insights into its structural performance. The load–deflection relationship confirms the cross-arm behaves as a linear elastic material, with the fixed point experiencing the least deflection and the free end the most. The inclusion of a plug-in type sleeve reinforcement significantly reduces deflection and enhances resistance to bending forces. At all critical observation points, the reinforced cross-arm shows a notably higher elastic modulus, indicating improved strength. The effectiveness of the reinforcement is clear as the sleeved cross-arm demonstrates approximately 29% lower deflection compared to the virgin version. Additionally, the reinforced cross-arm exhibits enhanced creep resistance and a shorter viscoelastic transition phase. Creep testing shows point Y3 undergoes the highest creep strain. With percentage errors below 5%, Findley's power law model effectively represents the creep behavior of both cross-arm types.

Projections indicate that after 50 years, the average elastic modulus would decrease by about 59% for the virgin cross-arm and 37% for the reinforced one. The sleeve structure improves the virgin PGFRP composite cross-arm by nearly 50%, boosting both strength and long-term durability. This research also

Table 9 Summary of life span prediction based on elastic moduli

Cross-arm	$E_{e,10\ years}$ (GPa)	$E_{e,25\ years}$ (GPa)	$E_{e,50\ years}$ (GPa)	$\chi_{50years}$	R^2
Virgin	134.08	120.27	109.97	0.41	0.9956
Sleeved	239.49	228.14	219.38	0.62	0.9957

provides a basis for further studies into possible limitations, such as stress concentrations in the inner walls due to sleeve insertion, the tribological properties of exposed versus unexposed regions, and the potential for dynamic failure. Overall, this study validates the improved creep performance of sleeve-reinforced PGFRP composite cross-arms. The structural enhancement proves effective in extending service life and improving mechanical reliability under real-world conditions. However, as this study did not explore environmental sustainability or economic feasibility, future research should include an evaluation of lifecycle impacts and material cost–benefit considerations.

Author contributions Vijayvignesh Namasivayam Sukumaar contributed to Conceptualization, Methodology, Data curation, Formal Analysis, Investigation, Writing—Original draft preparation, Writing—Reviewing and Editing. Mohamad Ridzwan Ishak assisted in Funding Acquisition, Visualization, Investigation, Supervision. Mohd Na'Im Abdullah provided Resources, Visualization, Validation. Mohamed Yusoff Mohd Zuhri supported in Visualization, Investigation, Software. Muhammad Asyraf Muhammad Rizal performed Validation, Methodology, Project Administration.

Funding Open access funding provided by The Ministry of Higher Education Malaysia and Universiti Putra Malaysia. This research work was funded by Universiti Putra Malaysia (UPM) for financial support under Geran Inisiatif Putra Siswazah (GP-IPS): GP-IPS/2023/9743400 to carry out all research activities. The authors are also very thankful to Department of Aerospace Engineering, Faculty of Engineering, UPM and Aerospace Malaysia Research Centre (AMRC), UPM for providing space and facilities for the project.

Data availability The data that support the findings of this study are available from the corresponding author upon request.

Declarations

Conflict of interest The authors declare that they have no known competing financial interests or personal relationships that could have appeared to influence the work reported in this paper.

References

1. A.L. Amir, M.R. Ishak, N. Yidris, M.Y.M. Zuhri, M.R.M. Asyraf, Potential of honeycomb-filled composite structure in composite cross-arm component: a review on recent progress and its mechanical properties. Polymers **13**, 1341 (2021). https://doi.org/10.3390/polym13081341
2. S.A. Rufus, N.A. Ahmad, N. Abdullah, Z. Abdul-Malek, A comparative analysis using machine learning approach for thunderstorm prediction in southern region of Peninsular Malaysia. Proc. Int. Symp. Lightning Prot. (XVII SIPDA) **2023**, 1–6 (2023). https://doi.org/10.1109/SIPDA59763.2023.10349193
3. N. Saleh, M. Gharaylou, M.M. Farahani, O. Alizadeh, Performance of lightning potential index, lightning threat index, and the product of CAPE and precipitation in the WRF model. Earth Space Sci. **10**, e2023EA003104 (2023). https://doi.org/10.1029/2023EA003104
4. P. Rajeev, S. Bandara, E. Gad, J. Shan, Structural assessment techniques for in-service crossarms in power distribution networks. Infrastructures **7**, 94 (2022). https://doi.org/10.3390/infrastructures7070094
5. J.S. Leon Colqui, M.R.A. de Ribeiro, S.M.A. De Oliveira, J.P. Filho, S. Kurokawa, The impact of transmission line modeling on lightning overvoltage. Energies **16**, 1343 (2023). https://doi.org/10.3390/en16031343
6. A. Mohamad, M.P. Yahaya, N.S. Hudi, Revised tower earthing design in high-voltage transmission network for high-frequency lightning condition. J. Phys. Conf. Ser. **1878**, 012005 (2021). https://doi.org/10.1088/1742-6596/1878/1/012005
7. N. Kumar, A.S. Joseph, P. Mehrotra, S.D. Yadav, An improved dislocation density reliant model to address the creep deformation of reduced activation ferritic martensitic steel. Forces Mech. **9**, 100117 (2022). https://doi.org/10.1016/j.finmec.2022.100117
8. M.R.M. Asyraf, M. Rafidah, M.R. Ishak, S.M. Sapuan, N. Yidris, R.A. Ilyas, M.R. Razman, Integration of TRIZ, morphological chart and ANP method for development of FRP composite portable fire extinguisher. Polym. Compos. **41**, 2917–2932 (2020). https://doi.org/10.1002/pc.25587
9. N. Roslan, U.A.U. Amirulddin, M.Z.A. Ab Kadir, N. Abdullah, Development of GIS-based ground flash density and its statistical analysis for lightning performance evaluation of transmission lines in Peninsular Malaysia. Pertanika J Sci Technol (2024). https://doi.org/10.47836/pjst.32.1.21
10. H. Wang, Q. Deng, X. Wang, L. Chen, Research on the crashworthiness of composite foam gradient-reinforced carbon fiber tubes. Fibers Polym. **25**(7), 2741–2750 (2024). https://doi.org/10.1007/s12221-024-00618-0
11. T.Y. Su, S.B. Yaakob, A.M. Ariffen, Modelling and analysis of electrical performance outdoor glass insulator under various services and lightning impulse. J. Phys. Conf. Ser. **2550**(1), 012021 (2023). https://doi.org/10.1088/1742-6596/2550/1/012021
12. M.R.M. Asyraf, M. Rafidah, E. Madenci, Y.O. Özkılıç, C. Aksoylu, M.R. Razman, T. Khan, Creep properties and analysis of cross arms' materials and structures in latticed transmission towers: current progress and future perspectives. Materials **16**(4), 1747 (2023). https://doi.org/10.3390/ma16041747
13 A. Alhayek, A. Syamsir, V. Anggraini, Z.C. Muda, N.M. Nor, Numerical modelling of glass fiber reinforced polymer (GFRP) cross arm. Int. J. Recent Technol. Eng. **8**, 6484–6489 (2019). https://doi.org/10.35940/ijrte.d5162.118419
14. T. Nafo, G.S. Punekar, K. Ibrahim, M. Berhanu, Comparative analysis of 500 kV double-circuit transmission line electric field intensity: Ethiopian lines compliance with ICNIRP. IEEE Access (2024). https://doi.org/10.1109/ACCESS.2024.3406902

15 V. NamasivayamSukumaar, M.R. Ishak, M.N.I. Abdullah, M.Z. Mohamed Yusoff, M.A.M. Rizal, Experimental investigation of flexural mechanical and flexural creep properties of sleeved PGFRP composite used in transmission tower application. Glob Congr Manuf Manag (2023). https://doi.org/10.1007/978-3-031-80341-3_23
16. A. Alhayek, A. Syamsir, A.B.M. Supian, F. Usman, M.R.M. Asyraf, M.A. Atiqah, Flexural creep behaviour of pultruded GFRP composites cross-arm: a comparative study on the effects of stacking sequence. Polymers **14**, 1330 (2022). https://doi.org/10.3390/polym14071330
17. S.K. Kumar, M. Anbarasu, G.M. Ganesh, Flexural behaviour and design of hybrid cold-formed steel built-up I-section beams. Structures **69**, 107243 (2024). https://doi.org/10.1016/j.istruc.2024.107243
18. D. Betts, P. Sadeghian, A. Fam, Experimental and analytical investigations of the flexural behavior of hollow ±55 filament wound GFRP tubes. Thin-Walled Struct. **159**, 107246 (2021). https://doi.org/10.1016/j.tws.2020.107246
19. Z. Wang, K. Wang, J. Zhao, S. Wang, E.D. Shumuye, Z. Yang, The mechanical properties of GFRP bars embedded in geopolymer concrete after high temperature exposure. J. Build. Eng. **62**, 105355 (2022). https://doi.org/10.1016/j.jobe.2022.105355
20. D.C.T. Cardoso, K.A. Harries, A viscoelastic model for time-dependent behavior of pultruded GFRP. Constr. Build. Mater. **208**, 63–74 (2019). https://doi.org/10.1016/j.conbuildmat.2019.02.155
21. M.R.M. Asyraf, M.R. Ishak, S.M. Sapuan, N. Yidris, Influence of additional bracing arms as reinforcement members in wooden timber cross-arms on their long-term creep responses and properties. Appl. Sci. **11**, 2061 (2021). https://doi.org/10.3390/app11052061
22. M.R.M. Asyraf, M.R. Ishak, S.M. Sapuan, N. Yidris, Utilization of bracing arms as additional reinforcement in pultruded glass fiber-reinforced polymer composite cross-arms: creep experimental and numerical analyses. Polymers **13**, 620 (2021). https://doi.org/10.3390/polym13040620
23. M.S. Abu Bakar, A. Syamsir, A. Alhayek, M.R.M. Asyraf, Z. Itam, S.M.M. Shaik, N.A. Aziz, T. Jamal, S.A. MohdMansor, The reduction factor of pultrude glass fibre-reinforced polyester composite cross-arm: A comparative study on mathematical modelling for life-span prediction. Materials **16**, 5328 (2023). https://doi.org/10.3390/ma16155328
24. H.K. Sharaf, M.R. Ishak, S.M. Sapuan, N. Yidris, Conceptual design of the cross-arm for the application in the transmission towers by using TRIZ–morphological chart–ANP methods. J. Mater. Res. Technol. **9**, 9182–9188 (2020). https://doi.org/10.1016/j.jmrt.2020.05.129
25. A.L. Amir, M.R. Ishak, N. Yidris, M.Y.M. Zuhri, M.R.M. Asyraf, M.R. Razman, Z. Ramli, Full-scale evaluation of creep coefficients and viscoelastic moduli in honeycomb sandwich pultruded GFRP composite cross-arms: Experimental and numerical study. Results Eng. **21**, 101850 (2024). https://doi.org/10.1016/j.rineng.2024.101850
26. A.L. Amir, M.R. Ishak, N. Yidris, M.Y.M. Zuhri, Flexural creep response of honeycomb sandwich pultruded GFRP composite cross-arm: obtaining full-scale viscoelastic moduli and creep coefficients. J. Mater. Res. Technol. **29**, 225–241 (2024). https://doi.org/10.1016/j.jmrt.2024.01.091
27. A.M. Bell, N. Keltsch, P. Schweyen, G. Reifferscheid, T. Ternes, S. Buchinger, UV aged epoxy coatings—Ecotoxicological effects and released compounds. Water Res. X **12**, 100105 (2021). https://doi.org/10.1016/j.wroa.2021.100105
28. N.G. Leiva, R.A. Herrera, L.M. Massone, J.F. Beltrán, Numerical modeling of beam plastic hinges in steel moment resisting frames including local buckling and stiffness/strength degradation. Structures **69**, 107260 (2024). https://doi.org/10.1016/j.istruc.2024.107260
29. C. Ji, H. He, Y. Yang, Moisture absorption process of epoxy resin and mechanical properties of its fiber composites. Mater. Test. **61**, 23–26 (2019). https://doi.org/10.3139/120.111276
30. L. Cao, L. Guo, M. Dhanasekar, Development of a new outer sleeve assembly for beam-column connections. J. Constr. Steel Res. **164**, 105769 (2020). https://doi.org/10.1016/j.jcsr.2019.105769
31. Y. Liu, X. Li, X. Zheng, Z. Song, Experimental study on seismic response of precast bridge piers with double-grouted sleeve connections. Eng. Struct. **221**, 111023 (2020). https://doi.org/10.1016/j.engstruct.2020.111023
32. P. Zhang, J. Yu, Y. Pang, J. Fan, H. Guo, Z. Pan, Experimental study on the mechanical properties of grouted sleeve joint with the fiber-reinforced grouting material. J. Build. Eng. **41**, 102691 (2021). https://doi.org/10.1016/j.jobe.2021.102691
33. D.K. Rajak, P.H. Wagh, H. Moustabchir, C.I. Pruncu, Improving the tensile and flexural properties of reinforced epoxy composites by using cobalt filled and carbon/glass fiber. Forces Mech **4**, 100029 (2021). https://doi.org/10.1016/j.finmec.2021.100029
34. K. Cheng, Y. Wang, H. Fang, C. Qian, P. Wu, Experimental investigation and prediction for bending creep of glass fiber-reinforced polymer pultruded tube. Buildings **13**, 2714 (2023). https://doi.org/10.3390/buildings13112714
35. V.N. Sukumaar, M.R. Ishak, M. Na'Im Abdullah, M.Y.M. Zuhri, M.A.M. Rizal, Experimental investigation and theoretical prediction of sleeve reinforced PGFRP composite under flexural loading for cross-arm application. Results Eng **25**, 103735 (2025). https://doi.org/10.1016/j.rineng.2024.103735
36. M.M. Attia, M.M. Olwan, E. Amoush, S.R.R.H. Aamer, M.A. Eita, Behavior of hybrid natural fiber reinforced polymers bars under uniaxial tensile strength and pull-out loads with UHPC. Case Stud Constr Mater (2024). https://doi.org/10.1016/j.cscm.2024.e03442
37. D. Kukla, A. Kozlowski, I. Wójcik-Grząba, Ductility of the double-sided bolted steel end-plate joint with column web openings under column loss scenario. Structures **69**, 107264 (2024). https://doi.org/10.1016/j.istruc.2024.107264
38. X.T. Nguyen, J.S. Park, Design equations for buckling strength of steel I-beam under non-uniform heating condition. Fire Saf. J.Saf. J. **127**, 103464 (2022). https://doi.org/10.1016/j.firesaf.2021.103464
39. A.L. Amir, S. Yamunan, M.R. Ishak, N. Yidris, M.Y.M. Zuhri, Flexural creep behavior in utilization of woven glass-fibre as reinforcement in pultruded glass fibre-reinforced polymer composite cross-arms: experimental and numerical analysis. E3S Web Conf. **477**, 00007 (2024). https://doi.org/10.1051/e3sconf/202447700007
40. T. Dhilipkumar, M. Vasumathi, S.R. Begum, P. Sathyaseelan, B.K. Gnanavel, A.A. Ghfar, Evaluation of acoustic and structural behavior of banana fiber reinforced polymer composites. Fibers Polym. **25**, 2303–2314 (2024). https://doi.org/10.1007/s12221-024-00582-9
41 C. Abhishek, N. Raghukiran, Residual stresses in 4D printed structures: A review on causes, effects, measurements, mitigations and its applications. Forces Mech. (2024). https://doi.org/10.1016/j.finmec.2024.100304
42. Y. Yang, X. Huang, F. Liao, Y. Chen, Q. Lin, Y. Wang, Flexural behavior of ultra-high-performance concrete (UHPC) encased concrete-filled steel tubular (CFST) beams. Structures **69**, 107259 (2024). https://doi.org/10.1016/j.istruc.2024.107259
43. D.P. Islami, A.F. Muzaqih, R. Adiputra, A.R. Prabowo, N. Firdaus, S. Ehlers, M. Braun, M. Jurkovič, D.F. Smaradhana, H.

Carvalho, Structural design parameters of laminated composites for marine applications: Milestone study and extended review on current technology and engineering. Results Eng. **24**, 103195 (2024). https://doi.org/10.1016/j.rineng.2024.103195
44. R. Kumar, A. Lal, B.M. Sutaria, Numerical and experimental investigation for flexural response of Kevlar short fiber tissue/carbon fiber belts toughened honeycomb sandwich plate. Forces Mech **12**, 100222 (2023). https://doi.org/10.1016/j.finmec.2023.100222
45. V. Namasivayam Sukumaar, S. Arjunan, L.N. Pandiaraj, A. Narayanan, Experimental investigation of 3D printed polylactic acid and polylactic acid–hydroxyapatite composite through material extrusion technique for biomedical application. J. Thermoplast. Compos. Mater. (2024). https://doi.org/10.1177/08927057241255883
46. R. Elayaraja, G. Rajamurugan, Performance of hybrid composites fabricated by flax/hemp fibers using wire mesh plain weaving techniques. Fibers Polym. (2024). https://doi.org/10.1007/s12221-024-00763-6
47 J. Li, X. Huan, S. Wang, Y. Sheng, D. Xu, Z. You, Performance of optimized composition of epoxy resin adhesive used in high friction surface treatment. Case Stud. Constr. Mater. (2024). https://doi.org/10.1016/j.cscm.2024.e03431
48. W. Li, X. Zhao, Y. Huang, Y. Ouyang, Y. Liu, Fabrication and mechanical properties of flax/basalt fibers-reinforced polypropylene thermoplastic composites hybridized at the yarn level. Fibers Polym. (2024). https://doi.org/10.1007/s12221-024-00782-3
49. D. Singhal, V. Narayanamurthy, Large and small deflection analysis of a cantilever beam. J. Inst. Eng. India Ser. A **100**, 83–96 (2019). https://doi.org/10.1007/s40030-018-0342-3
50 W. Wu, X. He, W. Yang, Z. Tang, H. Wang, M. Zhou, B. Wei, J. He, Investigation of long-term degradation of the interface in the anchorage zone of GFRP-RC beams. Case Stud. Constr. Mater. (2024). https://doi.org/10.1016/j.cscm.2024.e03399
51. D. Ussorio, M.S. Vaccaro, R. Barretta, R. Luciano, F.M. de Sciarra, Large deflection of a nonlocal gradient cantilever beam. Int. J. Eng. Sci. **206**, 104172 (2025). https://doi.org/10.1016/j.ijengsci.2024.104172
52. J. Hu, J. Peng, Y. Shao, J. Xue, J. Chen, J. Zhang, Y. Ding, Y. Yang, Investigating the influence of weight ratios of polyester fibers as an adhesive on mechanical and acoustic properties of glass fiber composite felts. Fibers Polym. **25**, 3079–3090 (2024). https://doi.org/10.1007/s12221-024-00629-x
53. P. Luo, C. Yang, T. Wang, Making ultra-thin high density fiberboard using old corrugated container with kraft lignin. Bioresour. **17**, 2696–2704 (2022). https://doi.org/10.15376/biores.17.2.2696-2704
54. S. Garriba, H.S. Jailani, C.A. Pandian, Characterization of mechanical, viscoelastic, thermal properties of epoxy/<i>mariscus ligularis</i> fiber composites. Fibers Polym. **25**, 3975–3994 (2024). https://doi.org/10.1007/s12221-024-00707-0
55. A. Jayswal, J. Liu, G. Harris, R. Mailen, S. Adanur, Creep behavior of 3D printed polymer composites. Polym. Eng. Sci. **63**, 3809–3818 (2023). https://doi.org/10.1002/pen.26486
56. A. Syamsir, L.W. Ean, M.R.M. Asyraf, A.B.M. Supian, E. Madenci, Y.O. Özkılıç, C. Aksoylu, Recent advances of GFRP composite cross arms in energy transmission tower: a short review on design improvements and mechanical properties. Materials **16**, 2778 (2023). https://doi.org/10.3390/ma16072778
57. M.S. Abu Bakar, A. Syamsir, A. Alhayek, M.R.M. Asyraf, Z. Itam, S.M.M. Shaik, S.A. Mohd Mansor, The reduction factor of pultrude glass fibre-reinforced polyester composite cross-arm: a comparative study on mathematical modelling for life-span prediction. Materials **16**, 5328 (2023). https://doi.org/10.3390/ma16155328
58. A. Alhayek, A. Syamsir, A.B.M. Supian, F. Usman, M.I. Najeeb, M.R.M. Asyraf, A mathematical model of flexural-creep behaviour for future service expectancy of a GFRP composite cross-arm with the influence of outdoor temperature. Fibers Polym. **24**, 2425–2437 (2023). https://doi.org/10.1007/s12221-023-00235-3
59. H. Lin, L. Fan, Z. Zhang, J. Yuan, H. He, J. Yu, K. Yang, Research on axial compressive performance of ceramic concrete reinforced with HTPP fibers. Case Stud. Constr. Mater. **21**, e03412 (2024). https://doi.org/10.1007/s12221-023-00235-3
60. H.A. Atar, M. Zarrebini, J. Rezaeepazhand, H. Hasani, The effect of structural integrity and geometric configurations of corrugated cores on flexural properties of sandwich panels: experimental and numerical method. Fibers Polym. **25**, 4371–4385 (2024). https://doi.org/10.1007/s12221-024-00725-y
61. M.R.M. Asyraf, A. Syamsir, H. Bathich, Z. Itam, A.B.M. Supian, S. Norhisham, M.Z.A. Rashid, Effect of fibre layering sequences on flexural creep properties of kenaf fibre-reinforced unsaturated polyester composite for structural applications. Fibers Polym. **23**, 3232–3240 (2022). https://doi.org/10.1007/s12221-022-4386-7
62. D. Mohamad, S. Beddu, A. Syamsir, N.M. Zahari, M.F. Razali, S.A.H.A. Seman, F.C. Ng, Failure analysis of various fiberglass cross-arm designs under multi-axial loading. IOP Conf. Ser. Mater. Sci. Eng. **920**, 012037 (2020). https://doi.org/10.1088/1757-899X/920/1/012037
63. Shah, D. U. Materials selection charts for designing products with biocomposites. (2020). https://doi.org/10.1016/B978-0-12-803581-8.11658-3
64. J. Zhao, M. Zhu, L. Xu, M. Shi, C. Wang, Experimental study on flexural properties of FRP foam sandwich plates in hot and humid environment. Fibers Polym. **25**, 2315–2325 (2024). https://doi.org/10.1007/s12221-024-00586-5
65. G. Ananth, S. Thirugnanam, S. Rajaram, Load-bearing and machining behavior of treated nano-sorghum-millet-husk-biosilica-and kenaf-fiber-reinforced vinyl ester composite. Fibers Polym. **25**, 4387–4399 (2024). https://doi.org/10.1007/s12221-024-00736-9
66. Z. Sajid, S. Karuppanan, N. Sallih, K.E. Kee, S.Z.H. Shah, Role of washer size in mitigating adverse effects of bolt-hole clearance in a single-lap, single-bolt basalt composite joint. Composite Struct **266**, 113802 (2021). https://doi.org/10.1016/j.compstruct.2021.113802
67. G.O.N.G. Hao, L.I.U. Jianhua, F.E.N.G. Huihua, Review on anti-loosening methods for threaded fasteners. Chinese J. Aeronaut. **35**, 47–61 (2022). https://doi.org/10.1016/j.cja.2020.12.038
68. Z. Fang, L. Hu, H. Jiang, S. Fang, G. Zhao, Y. Ma, Shear performance of high-strength friction-grip bolted shear connector in prefabricated steel–UHPC composite beams: finite element modelling and parametric study. Case Stud. Constr. Mater. **18**, e01860 (2023). https://doi.org/10.1016/j.cscm.2023.e01860
69. H.K. Sharaf, M.R. Ishak, S.M. Sapuan, N. Yidris, A. Fattahi, Experimental and numerical investigation of the mechanical behavior of full-scale wooden cross arm in the transmission towers in terms of load-deflection test. J. Mater. Res. Technol. **9**, 7937–7946 (2020). https://doi.org/10.1016/j.jmrt.2020.04.069
70. M.F. Abd El-Halim, M.M. Awd Allah, A.S. Almuflih, M.A. Abd El-baky, Axial crashworthiness characterization of bio-inspired 3D-printed gyroid structure tubes: cutouts effect. Fibers Polym. **25**, 3099–3114 (2024). https://doi.org/10.1007/s12221-024-00630-4
71. M.R.M. Asyraf, M.R. Ishak, S.M. Sapuan, N. Yidris, Comparison of static and long-term creep behaviors between balau wood and glass fiber reinforced polymer composite for cross-arm application. Fibers Polym. **22**, 793–803 (2021). https://doi.org/10.1007/s12221-021-0512-1

72 D. Liu, X. Feng, K. Duan, J. Zuo, G. Chen, M. Li, Z. Xia, A novel concrete-filled flange steel tubular composite supports for tunnels: a numerical perspective. Case Stud. Constr. Mater. (2024). https://doi.org/10.1016/j.cscm.2024.e03384

73. O. Singh, B.K. Behera, Mechanical performance of intralayer hybrid 3D woven honeycomb core for lightweight structural composites. Fibers Polym. **25**, 4401–4419 (2024). https://doi.org/10.1007/s12221-024-00743-w

74. Z. Zhou, X. Zhou, Modified plastic stress distribution method incorporating size effect for strength prediction of CFST members. Structures **70**, 107632 (2024). https://doi.org/10.1016/j.istruc.2024.107632

75. F. Gao, W.H. Liao, X. Wu, Being gradually softened approach for solving large deflection of cantilever beam subjected to distributed and tip loads. Mech. Mach. Theory **174**, 104879 (2022). https://doi.org/10.1016/j.mechmachtheory.2022.104879

76. M. Salah, A. Farag, H. Mostafa, A. Elansary, Flexural behavior of bonded post-tensioned concrete beams with steel or GFRP bars. Structures **70**, 107549 (2024). https://doi.org/10.1016/j.istruc.2024.107549

77. Y. Huang, J. Fu, R. Wang, R. Rao, N. Ma, Experimental study on creep behavior of high-strength concrete filled steel tubular (HSCFST) columns. Case Stud. Constr. Mater. **20**, e02690 (2024). https://doi.org/10.1016/j.cscm.2023.e02690

78. Y. Bai, J. Zhang, H. Shen, Residual compressive load-carrying capacity of cross-laminated timber walls after exposed to one-side fire. J. Build. Eng. **34**, 101931 (2021). https://doi.org/10.1016/j.jobe.2020.101931

79. A. Seif, S.F. Mahmoud, M. Megahed, Enhancement of impact, shear and wear performance of glass fiber/epoxy composites by inclusion of polycarbonate sheets. Fibers Polym. (2024). https://doi.org/10.1007/s12221-024-00757-4

80. X. Zhang, S. Yu, S. Feng, W. Huang, X. Li, Tensile behaviour of a novel grouted sleeve splice for high-strength rebars. Structures **70**, 107631 (2024). https://doi.org/10.1016/j.istruc.2024.107631

81. V. Daghigh, H. Edalati, H. Daghigh, D.M. Belk, K. Nikbin, Time-dependent creep analysis of ultra-high-temperature functionally graded rotating disks of variable thickness. Forces Mech. **13**, 100235 (2023). https://doi.org/10.1016/j.finmec.2023.100235

82. S.M. Hussnain, S.Z.H. Shah, P.S.M. Megat-Yusoff, M.Z. Hussain, Degradation and mechanical performance of fibre-reinforced polymer composites under marine environments: a review of recent advancements. Polym. Degrad. Stab. **215**, 110452 (2023). https://doi.org/10.1016/j.polymdegradstab.2023.110452

83. X. Qi, J. Tian, G. Xian, Hydrothermal ageing of carbon fiber reinforced polymer composites applied for construction: a review. J. Mater. Res. Technol. **27**, 1017–1045 (2023). https://doi.org/10.1016/j.jmrt.2023.09.198

84. R. Wang, M. Yue, Y. Xiong, J. Yue, Experimental study on mechanism, aging, rheology and fatigue performance of carbon nanomaterial/SBS-modified asphalt binders. Constr. Build. Mater. **268**, 121189 (2021). https://doi.org/10.1016/j.conbuildmat.2020.121189

85. H. Cheng, P. Chen, S. Cao, Y. Li, Stress–strain model of steel fibre-reinforced alkali-activated slag cementitious material after high-temperature exposure. J. Build. Eng. **79**, 107743 (2023). https://doi.org/10.1016/j.jobe.2023.107743

86. M.M. Awd Allah, M.A. Abbas, A.S. Almuflih, S.F. Mahmoud, M.A. Abd El-baky, On the influence of different infill pattern structures on the crashworthiness performance of 3D printed tubes subjected to lateral loading condition. Fibers Polym. **25**, 4437–4451 (2024). https://doi.org/10.1007/s12221-024-00756-5

87. F. Wang, X. Bai, Z. Wu, N. Yan, D. Hou, J. Liu, Field pullout test and anchorage length calculation for external anchorage of GFRP anti-floating anchors. Structures **70**, 107636 (2024). https://doi.org/10.1016/j.istruc.2024.107636

88. ASTM-D2990 standard test methods for tensile, compressive, and flexural creep and creep-rupture of plastics, *Annual Book ASTM Standards* **I**, 1–20 (2017).

89. K. Zhao, J. Chen, M. Gao, G. You, X. Gao, Research of extreme service temperature on the bending behavior of composites for wind turbine blades. Fibers Polym. **25**, 2733–2740 (2024). https://doi.org/10.1007/s12221-024-00599-0

90. M. Zawam, K. Soudki, J.S. West, Factors affecting the time-dependent behaviour of GFRP prestressed concrete beams. J. Build. Eng. **24**, 100715 (2019). https://doi.org/10.1016/j.jobe.2019.02.007

91. C. Dong, Optimal design of carbon and glass reinforced hybrid composite pipes under flexural loading. Forces Mech **2**, 100003 (2021). https://doi.org/10.1016/j.finmec.2020.100003

92. N.R. Prakash, C. Gnanavel, Investigation of quartz-rich granite dust particle-reinforced aluminized glass–kenaf fiber-reinforced polyester composite: load bearing, water absorption and flame properties. Fibers Polym. **25**, 3525–3537 (2024). https://doi.org/10.1007/s12221-024-00671-9

93. F. Hoseinzadeh, S.M. Zabihzadeh, F. Dastoorian, Creep behavior of heat treated beech wood and the relation to its chemical structure. Constr. Build. Mater. **226**, 220–226 (2019). https://doi.org/10.1016/j.conbuildmat.2019.07.181

94. Q. Pei, Y. Zhong, B. Wang, P. Qi, Z. Xue, D. Cui, B. Cai, Performance of SRC unequal-depth beam-column irregular joint in NPP under progressive collapse. Structures **70**, 107593 (2024). https://doi.org/10.1016/j.istruc.2024.107593

95. F. Hasanalizadeh, H. Dabiryan, Investigation into the role of Z-fiber orientation in low-velocity impact behavior of sandwich-structured composite: numerical and experimental analysis. Fibers Polym. **25**, 4807–4822 (2024). https://doi.org/10.1007/s12221-024-00732-z

96. V. Gribniak, H.A. Sultani, A. Rimkus, R. Boris, A. Sokolov, L. Torres, Quantifying the flexural stiffness changes in the concrete beams with externally bonded carbon fiber sheets under elevated environment temperature. Alexandria Eng. J. **104**, 688–700 (2024). https://doi.org/10.1016/j.aej.2024.08.044

97. Y. Chen, Y. Xu, G. Yang, S. Wang, Z. Hu, H. Zhao, J. Liu, Research on creep behaviour of UHPC based on experiments and viscoelastic modelling. J. Build. Eng. **84**, 108585 (2024). https://doi.org/10.1016/j.jobe.2024.108585

98. M. Saadatfar, M.A. Babazadeh, M. Babaelahi, Coupled thermo-mechanical analysis of creep in a rotating FGMEE annular plate under complex thermal loading considering solar radiation, convection, and internal heat source. Forces Mech **16**, 100277 (2024). https://doi.org/10.1016/j.finmec.2024.100277

99. R. Tomisawa, Y. Ohkoshi, K. Kim, Thickness and compression behavior of a nonwoven produced by melt-blowing a polypropylene/poly (ethylene terephthalate) fiber mix. Fibers Polym. **25**, 3539–3548 (2024). https://doi.org/10.1007/s12221-024-00643-z

100. T. D'Antino, M.A. Pisani, Long-term behavior of GFRP reinforcing bars. Compos. Struct. **227**, 111283 (2019). https://doi.org/10.1016/j.compstruct.2019.111283

101. Z. Cai, X. Duan, L. Liu, Z. Lu, J. Ye, Reinforced ultra-high performance concrete beam under flexure and shear: experiment and theoretical model. Case Stud. Constr. Mater. **20**, e02647 (2024). https://doi.org/10.1016/j.cscm.2023.e02647

102. C.B. Ayyanar, R. Kumar, S. Helaili, B. Gayathri, T. Bal, F. Gapsari, S. Siengchin, Experimental and numerical analysis of natural fillers loaded and E-glass reinforced epoxy sandwich composites. J. Mater. Res. Technol. **32**, 1235–1244 (2024). https://doi.org/10.1016/j.jmrt.2024.07.142

103. Q.X. Ren, K. Zhou, W. Li, Experimental study of clay concrete filled steel tubular stub columns under axial compression. Structures **70**, 107509 (2024). https://doi.org/10.1016/j.istruc.2024.107509

104. S. Bhattacharya, K. Kalita, R. Čep, S. Chakraborty, A comparative analysis on prediction performance of regression models during machining of composite materials. Materials **14**(21), 6689 (2021). https://doi.org/10.3390/ma14216689
105. Y. Xia, X. Li, T. Xie, R. Zhu, G. Wang, G. Yi, J. Li, Seismic performance of RC bent columns: experimental, numerical and life-cycle cost analysis. Case Stud. Constr. Mater. **20**, e02692 (2024). https://doi.org/10.1016/j.cscm.2023.e02692